Homoclinic Bifurcations for the Hénon Map

D. Sterling, H.R. Dullin & J.D. Meiss *
Department of Applied Mathematics
University of Colorado
Boulder, CO 80309

October 5, 1998

Abstract

Chaotic dynamics can be effectively studied by continuation from an anti-integrable limit. We use this limit to assign global symbols to orbits and use continuation from the limit to study their bifurcations. We find a bound on the parameter range for which the Hénon map exhibits a complete binary horseshoe as well as a subshift of finite type, and study these numerically. We classify homoclinic bifurcations, and study those for the area-preserving case in detail. Simple forcing relations between homoclinic orbits are established. We show that a symmetry of the map gives rise to constraints on certain sequences of homoclinic bifurcations. Our numerical studies of the number of periodic orbits confirm and extend the results of Davis, MacKay and Sannami.
AMS classification scheme numbers: 58F05, 58F03, 58C15

1 Introduction

The problem of determining the sequence of bifurcations that result in the creation of a Smale horseshoe is an interesting one [1, 2, 3]. In this paper we use a continuation technique based on an "anti-integrable" (AI) limit [4] to study some of these bifurcations from the opposite side, that is, as bifurcations that destroy the horseshoe.

As a simple example, we study the two parameter Hénon family of maps

$$\begin{pmatrix} x' \\ y' \end{pmatrix} = \begin{pmatrix} y - k + x^2 \\ -bx \end{pmatrix}. \tag{1}$$

As we recall in §2, the AI limit for this map is essentially $k \to \infty$. In order to represent this with finite parameters, we need only rescale the map, letting

*Useful conversations with R. Easton and B. Peckham are gratefully acknowledged. JDM was supported in part by NSF grant number DMS-9623216. HRD was supported by DFG grant number Du 302/1

$z = \epsilon x$, where

$$\epsilon = \frac{1}{\sqrt{k}}\,.$$

As was shown by Devaney and Nitecki [5], the Hénon map has a hyperbolic horseshoe when

$$k > (1+b^2)\frac{5+2\sqrt{5}}{4}\,. \tag{2}$$

The Hénon map has at most 2^n fixed points of period n, and when the map has a hyperbolic horseshoe, all these orbits exist and are easily identified by their symbolic labels.

We showed earlier [6] that a contraction mapping argument implies there is a one-to-one correspondence between orbits in the AI limit and bounded orbits of the Hénon map in precisely the range Eq. (2). In §5 we show that this result can be easily extended for a particular subset of the orbits. Moreover, in §6, we present results of numerical investigations that tighten these bounds to what we believe are their optimal values.

In general, the existence of an anti-integrable limit leads to a natural symbolic characterization of orbits—for the Hénon map this is the same as the horseshoe coding. We use this coding, and as discussed in §3, a predictor-corrector continuation method [7], to give each orbit a *global code*. That is, we label an orbit with the AI code, and use this designation up to the maximal value of ϵ for which the orbit exists. For the Hénon map, this gives a correspondance between bounded orbits of the map and sequences of symbols $\mathbf{s} \in 2^{\mathbb{Z}}$, providing only that every orbit can be continuously connected to the AI limit. This hypothesis, which we call the "no-bubbles" hypothesis, is essential to our method. It is certainly valid when the hyperbolic horseshoe exists, but we know of no more general proof.

Our global code contrasts with other methods for constructing symbolic dynamics for maps, which rely on some attempt to obtain a generating partition for the map [8, 2, 9, 10, 11]. These methods rely on somewhat ad hoc techniques for constructing the partition, especially when there exist elliptic orbits. Our method gives a natural partition that is continuously connected to the horseshoe, though it does rely on the no-bubbles hypothesis.

In our computations of the Hénon map, we observe that the horseshoe destroying bifurcation appears to be a homoclinic saddle-node bifurcation when the map is orientation preserving, and a heteroclinic saddle-node when it is not. In §7 we study in detail the homoclinic orbits of the area-preserving Hénon map, and show how the AI code directly gives other properties of the orbits, such as their "type," "transition time," and "Poincaré signature."

For an area-preserving map, the destruction of a horseshoe by a homoclinic bifurcation gives rise generically to elliptic orbits. Specifically, if f is a C^1 area-preserving diffeomorphism with a homoclinic tangency at x then for any neighborhood U of x, there is an area preserving diffeomorphism C^1-close to f which has an elliptic periodic point in U [12].

Much more is known about the behavior of area-contracting maps near a homoclinic tangency. Gavrilov and Silnikov proved that if a C^3 map has a quadratic homoclinic tangency at a parameter k^* then there exists a sequence of parameter values $k_n \to k^*$ such that at k_n there is a saddle-node bifurcation creating orbits of period n [13, 14]; because one of the created orbits is a sink, this is called a *cascade of sinks*. Robinson extended these results for the real analytic case where the intersection is created degenerately [15]. In our computations we will find a similar cascade of saddle-node bifurcations for the area-preserving Hénon map—this gives a sequence of elliptic orbits that limit on the homoclinic bifurcation. Thus the destruction of the horseshoe is associated with the creation of the first stable "island."

The ordering on the invariant manifolds poses severe restrictions on the possible bifurcations. In §8 we use it to prove which homoclinic bifurcation of the hyperbolic fixed point is the first one. We observe that the forcing relations between homoclinic orbits up to type 6 is essentially like the unimodal ordering of one dimensional maps. Generically a homoclinic bifurcation corresponds to a quadratic tangency of the stable and unstable manifolds—a "homoclinic saddle-node bifurcation." There are two more generic bifurcations in maps with a symmetry: a homoclinic pitchfork when the manifolds exhibit a cubic tangency, and a simultaneous pair of asymmetric saddle node bifurcations. In §9 we show that a symmetric homoclinic bifurcation forbids certain other bifurcation to occur after it, leading to a natural mechanism to create homoclinic pitchfork bifurcations or asymmetric saddle node pairs. We observe all three of these bifurcations for the area-preserving Hénon map, which has a time-reversal symmetry.

Davis, MacKay, and Sannami [3] conjectured that there are intervals of k below the horseshoe for which the Hénon map is a hyperbolic Markov shift. They also identified the Markov partitions for these cases. Their conjecture was based on computing all the periodic orbits up to a period 20 using the technique of Biham and Wenzel [16, 17]. In §10, we confirm their computations with our continuation technique and extend them to period 24—an order of magnitude more orbits. Moreover, we identify the bifurcations responsible for the creation and destruction of these apparently hyperbolic intervals; as befits with the theme of this paper, they are homoclinic bifurcations.

2 Anti-Integrable Limit

Dynamics in discrete time can be represented by a relation, $F(x, x') = 0$ where x and x' are points in some manifold. Normally, we can explicitly solve for $x' = f(x)$, giving a map on the manifold, with orbits defined by sequences $x_t = f(x_{t-1})$. Suppose, however, that F depends upon a parameter ϵ, in such a way that this is not always possible; for example, $F(x, x') = \epsilon G(x, x') + H(x)$. In this case the implicit equation $F = 0$ can no longer be solved for x' when $\epsilon = 0$; instead "orbits" correspond to

arbitrary sequences of points, x_t that are zeros of H—the dynamics are not deterministic. In this case we say that $\epsilon = 0$ corresponds to an *anti-integrable limit (AI)* of the map f [18]. If the derivative of H is nonsingular, then a straightforward implicit function argument can be used to show that the AI orbits can be continued for $\epsilon \neq 0$ to orbits of the map f [4, 19]. An AI limit with this property is called *nondegenerate*.

For example, consider the Hénon map Eq. (1). Denoting points on an orbit by a sequence $x_t, t \in \mathbb{Z}$, we can rewrite Eq. (1) as a second order difference equation

$$x_{t+1} + bx_{t-1} + k - x_t^2 = 0.$$

Introducing the scaled coordinate $z = \epsilon x$ and choosing $\epsilon = k^{-1/2}$ gives an implicit map in the variable z with parameter ϵ

$$\epsilon(z_{t+1} + bz_{t-1}) + 1 - z_t^2 = 0\,. \tag{3}$$

With this choice of ϵ, we can study only the range $0 < k < \infty$; however, one could redefine ϵ to shift this range [1].

In the AI limit, the map Eq. (3) reduces to

$$z_t^2 = 1\,.$$

Thus "orbits" in this limit are arbitrary sequences of ± 1, which we abbreviate with $+$ and $-$. Let Σ denote the space of such sequences

$$\Sigma \equiv \{-,+\}^{\mathbb{Z}} = \{\mathbf{s} : s_t \in \{-,+\}\,, t \in \mathbb{Z}\}\,. \tag{4}$$

It is often convenient to make Σ a metric space by mapping the symbols to $\{0,1\}$ respectively and using the metric

$$\rho(\mathbf{s},\mathbf{t}) \equiv \sum_{j=-\infty}^{\infty} \frac{|s_j - t_j|}{2^{|j|}}\,,$$

for any two sequences $\mathbf{s}, \mathbf{t} \in \Sigma$.

For ease of notation we denote the corresponding sequence of $\{+1,-1\} \in \mathbb{R}^{\mathbb{Z}}$ by the same symbol $\mathbf{s}$. Hence every sequence $\mathbf{s} \in \Sigma$ is an orbit $\mathbf{s} \in \mathbb{R}^{\mathbb{Z}}$ in the anti-integrable limit, and each of these can be continued to an orbit of the Hénon map for small enough ϵ [20, 19]. Previously we gave an explicit upper bound on ϵ for the existence of orbits for every symbol sequence [6]:

Theorem 1. *For every symbol sequence* $\mathbf{s} \in \Sigma$ *there exists a unique orbit* $\mathbf{z}(\epsilon)$ *of the Hénon map Eq. (3), such that* $\mathbf{z}(0) = \mathbf{s}$ *providing*

$$|\epsilon|(1 + |b|) < 2\sqrt{1 - 2/\sqrt{5}} \approx 0.649839\,. \tag{5}$$

[1] For example, choosing $\epsilon = (k+\delta)^{-1/2}$, maps positive values of ϵ to the range $-\delta < k < \infty$. Our numerical routines typically use $\delta = 1$ so that we can cover the entire parameter range where there are bounded orbits.

The basic idea of the proof of this theorem is as follows [6]. Let B_M be the closed ball of radius M around the point $\mathbf{s} \in \Sigma$,

$$B_M(\mathbf{s}) = \{\mathbf{z} : ||\mathbf{z} - \mathbf{s}||_\infty \leq M\}\,. \tag{6}$$

For each symbol sequence $\mathbf{s} \in \Sigma$ and small enough M, define a map $\mathbf{T} : B_M \to B_M$ by

$$T_i(\mathbf{z}) \equiv s_i \sqrt{1 + \epsilon(z_{i+1} + b z_{i-1})}\,. \tag{7}$$

Then the corresponding Hénon map orbit $\mathbf{z}(\epsilon)$ is a fixed point of $\mathbf{T}$. The conclusion of Thm. 1 follows from finding the maximum value of ϵ for which there is an n such that $\mathbf{T}^n$ is a contraction mapping (i.e., $\mathbf{T}^n : B_M \to B_M$ and $||DT^n|| < 1$).

The main point of the theorem is that there are no bifurcations in the range Eq. (5). In §6 we will use numerical continuation to estimate the parameters at which the first bifurcation occurs, giving an improvement in this bound, albeit a numerical one.

It is interesting that Devaney and Nitecki [5] obtained precisely the same bound, Eq. (5), for the domain in which the non-wandering set of the Hénon map is a hyperbolic horseshoe. Nevertheless the AI continuation argument has has two advantages over the geometrical arguments of Devaney and Nitecki. First, it easily generalizes to higher dimensions allowing one to compute parameter bounds for the existence of horseshoes in higher dimensional maps [21]. Second, it allows us to easily bound the parameter range for which certain subsets of orbits exist (i.e. the parameter range where the map is conjugate to a subshift of finite type). We present such a bound on the subshift of finite type in §5.

3 Numerical Method

In this section we formulate the problem of following Hénon map orbits away from the anti-integrable limit as a classical continuation problem [22].

A period n orbit of the Hénon map is given by a sequence $z_0, z_2, \ldots, z_{n-1}$ that satisfies Eq. (3), together with the condition that $z_{t+n} = z_t$. Formally we can write this as a single function $\mathbf{G} : \mathbb{R}^n \times \mathbb{R} \to \mathbb{R}^n$ whose t^{th} component is given by the left hand side of Eq. (3). We say that a sequence $\mathbf{z}(\epsilon) \equiv (z_0, z_2, \ldots, z_{n-1})^\infty$ is a period n orbit of the Hénon map with corresponding symbol sequence $\mathbf{s}$ if $\mathbf{z}(\epsilon)$ is a continuous function on some closed interval $\epsilon \in [0, \epsilon_{\max}]$ that satisfies

$$\begin{cases} \mathbf{G}(\mathbf{z}, \epsilon) &= \mathbf{0} \\ \mathbf{z}(0) &= \mathbf{s} \end{cases}\,.$$

Given an anti-integrable symbol sequence $\mathbf{s}$ and fixed ϵ, we continue $\mathbf{z}(0)$ away from the anti-integrable limit to locate the corresponding Hénon map

orbit $\mathbf{z}(\epsilon)$. This is a standard continuation problem, which we solve using a predictor-corrector method with a linear tangent predictor and a Newton's method corrector. The algorithm incorporates an adaptive step size control with bisection backtracking if the corrector fails to converge. The algorithm terminates when a user-specified value of ϵ is reached or, when the tangent direction is not uniquely defined. The process of continuing a sequence of orbits is trivially parallelizable since the operations performed on each orbit are completely independent of each other. We use a "divide and conquer" strategy to spread the total computational effort across several different machines running simultaneously. This is especially advantageous when the number of orbits continued reaches into the millions.

In the sections below we discuss the results obtained by using this method.

4 Symbolic Dynamics

In this section we introduce some notation for symbol sequences and bifurcations. For simplicity we concentrate mostly on the area-preserving case, $b = 1$, though many results apply generally.

Orbits in the anti-integrable limit are bi-infinite sequences $\mathbf{s} \in \Sigma$. When it is needed, we will indicate the current time along an orbit using a "$\bullet$", so that $\mathbf{s} = \ldots s_{-2}s_{-1} \bullet s_0 s_1 s_2 \ldots$. The dynamics on $\mathbf{s} \in \Sigma$ are given by the shift map, $\sigma : \Sigma \to \Sigma$ defined as

$$\sigma(\ldots s_{-1} \bullet s_0 s_1 s_2 \ldots) = \ldots s_{-1} s_0 \bullet s_1 s_2 \ldots$$

An orbit of the symbolic dynamics is periodic if the sequence $\mathbf{s}$ is periodic. We will denote an orbit of least period n by the string of n symbols and a superscript ∞ to represent repetition:

$$(s_0 s_1 \ldots s_{n-1})^\infty = \ldots s_{n-2} s_{n-1} \bullet s_0 s_1 \ldots s_{n-1} s_0 \ldots$$

Of course any cyclic permutation of a periodic orbit gives another point on the same orbit.

Trivially, the map σ has two fixed points, $(+)^\infty$ and $(-)^\infty$, and these correspond to the two fixed points of the Hénon map. These are born in a saddle-node bifurcation at $k = -(1+b)^2/4$, which we denote by

$$\mathrm{sn}\left\{(+)^\infty, (-)^\infty\right\}.$$

We denote bifurcations with the general template

$$\mathit{parent} \to \mathit{type}\left\{\mathit{children}\right\},$$

where *parent* refers to the orbit that is undergoing the bifurcation, if any, and *type* is one of sn, pf, pd, or m/n, corresponding to a saddle-node, pitchfork, period doubling, or rotational bifurcation, respectively. The set of orbits created in the bifurcation is listed as the *children*. When the

stability of these differ, we adopt the convention that the unstable child is listed first, and the stable one second.

When $b = 1$ the fixed points of the Hénon map are located at

$$z_\pm = \pm\sqrt{1+\epsilon^2} + \epsilon = \sqrt{k} \pm \sqrt{1+k}\,.$$

The stability of a period n orbit of an area preserving map f is conveniently classified by the "residue" defined as

$$R = \frac{1}{4}\left(2 - \mathrm{Tr}(Df^n)\right)\,,$$

so that an orbit is hyperbolic if it has negative residue, elliptic when $0 < R < 1$ and is reflection hyperbolic when $R > 1$ [23]. The residues of the fixed points are

$$R_\pm = \mp\frac{1}{2\epsilon}\sqrt{1+\epsilon^2} = \mp\frac{1}{2}\sqrt{1+k}\,, \tag{8}$$

so the sign of the symbol is opposite to the sign of the residue of the fixed point. Thus the orbit $(+)^\infty$ is always hyperbolic, while the orbit $(-)^\infty$ is reflection hyperbolic for small ϵ, or large k, but becomes elliptic at $\epsilon = 1/\sqrt{3}$, or $k = 3$.

The sequence $(+-)^\infty$ corresponds to the period two orbit

$$(+-)^\infty \;:\; (z_0, z_1) = (\sqrt{1-3\epsilon^2} - \epsilon, -\sqrt{1-3\epsilon^2} - \epsilon)\,.$$

This orbit exists only for $\epsilon < 1/\sqrt{3}$, and is created by a period doubling of the elliptic fixed point (when $R_- = 1$). We denote this bifurcation by

$$(-)^\infty \to \mathrm{pd}\,\{(+-)^\infty\}\,.$$

Similarly there are two period three orbits,

$$\begin{aligned}(--+)^\infty &: (z_0, z_1, z_2) = (-\sqrt{1-\epsilon^2}, -\sqrt{1-\epsilon^2}, \sqrt{1-\epsilon^2} - \epsilon)\\ (-++)^\infty &: (z_0, z_1, z_2) = (-\sqrt{1-\epsilon^2} - \epsilon, \sqrt{1-\epsilon^2}, \sqrt{1-\epsilon^2})\,.\end{aligned}$$

These are created in a saddle-node bifurcation at $\epsilon = 1$;

$$\mathrm{sn}\,\{(--+)^\infty, (-++)^\infty\}\,.$$

We list the low period orbits and their bifurcation values in Table 1. Another class of bifurcations shown in the table are rotational bifurcations. A rotational bifurcation occurs when the winding number of an elliptic orbit becomes $\omega = m/n$; we denote such bifurcations by the winding number of the parent orbit. For example the birth of orbits with winding number $1/n$ at the fixed point $(-)^\infty$ is denoted

$$(-)^\infty \to 1/n\,\{(--+^{n-2})^\infty, (-++^{n-2})^\infty\}\,. \tag{9}$$

Parent	Type	Child	Child	k-Value
	sn	$(-)^\infty$	$(+)^\infty$	-1
$(-)^\infty$	pd		$(+-)^\infty$	3
	sn	$(-+-)^\infty$	$(+-+)^\infty$	1
$(-)^\infty$	1/3	$(-+-)^\infty$		$\frac{5}{4}$
$(-)^\infty$	1/4	$(+--+)^\infty$	$(+-++)^\infty$	0
$(+-)^\infty$	pd		$(-+--)^\infty$	4
$(-)^\infty$	1/5	$(-++-+)^\infty$	$(++-++)^\infty$	$\frac{7-5\sqrt{5}}{8}$
$(-)^\infty$	2/5	$(--+--)^\infty$	$(-+-+-)^\infty$	$\frac{7+5\sqrt{5}}{8}$
	sn	$(+-+-+)^\infty$	$(+---+)^\infty$	5.5517014†
$(-)^\infty$	1/6	$(-+^4-)^\infty$	$(++-+^3)^\infty$	$-\frac{3}{4}$
$(+-+)^\infty$	pd		$(+-^4+)^\infty$	$\frac{5}{4}$
$(+-^4+)^\infty$	pf	$(++-+--)^\infty$	$(--+-++)^\infty$	3
	sn	$(--+-+-)^\infty$	$(--+-^3)^\infty$	3.7016569‡
$(+-)^\infty$	1/3	$(--+-+-)^\infty$		$\frac{15}{4}$
	sn	$(+-+^3-)^\infty$	$(--+^3-)^\infty$	5.6793695‡

† $16k^5 - 108k^4 + 105k^3 + 27k^2 - 97k - 47$

‡ $16k^6 - 136k^5 + 213k^4 + 220k^3 + 126k^2 + 108k + 81$

Table 1: Periodic orbits of the Hénon map up to period 6 and their bifurcations when $b = 1$. In the "type" column, "sn" indicates a saddle-node bifurcation, "pf" a pitchfork bifurcation, and "pd" a period doubling bifurcation. A rotational bifurcation is denoted by m/n, referring to the winding number of the parent at the bifurcation. For 1/3 the child is not created in the bifurcation, it exists before and after the bifurcation. If there are two children, the one listed in the first column has negative residue just after birth (except for the pf case). The real roots of the polynomials in the last rows give exact bifurcation values for the three approximations shown.

This particular rotational bifurcation occurs when the multipliers of the fixed point are $e^{i2\pi\omega}$ or using Eq. (8), when k is given by

$$k_\omega = \cos(2\pi\omega)(\cos(2\pi\omega) - 2)\,. \tag{10}$$

We have empirically identified the symbol sequences for rotational bifurcations, and will present the general symbolic formula for these and for rotational "islands around islands" orbits in [21].

The residue of any periodic orbit of a Lagrangian system is easily computed from the matrix M formed from the second variation of the action [24]. For a period n orbit of the Hénon map this formula gives:

$$R(z(\epsilon)) = -\frac{1}{4}\frac{\det(M)}{\epsilon^n}\,,$$

where M is the periodic tridiagonal matrix with elements elements

$$M_{t,t-1} = -b\epsilon\,, \quad M_{t,t} = 2z_t(\epsilon)\,, \quad M_{t,t+1} = -\epsilon\,.$$

As we approach the anti-integrable limit, $\mathbf{z}(\epsilon) \to \mathbf{s}$ as $\epsilon \to 0$ and M approaches the diagonal matrix $\mathrm{Diag}(2s_i)$. Thus we see that the residue becomes infinite at the anti-integrable limit and its sign is given by $-\prod_{t=0}^{n-1} s_t$. Hence,

$$\mathrm{sign}(R(\mathbf{s})) = -(-1)^j\,, \tag{11}$$

where j is the number of $-$'s in the symbol sequence $\mathbf{s}$.

5 A Subshift of Finite Type

In this section, we extend Thm. 1 to the case of a subshift of finite type. In particular, the biggest restriction in the proof of the theorem arises from the fact that the bounds on the operator $\mathbf{T}$ given in Eq. (7) are weakest when the signs $s_{i+1} = s_{i-1} = -1$. We can improve the bound by restricting the set of admissible symbol sequences to forbid this particular case. The shift map restricted to this subspace is a subshift of finite type with the forbidden set $\mathcal{F} = \{-+-, --- \}$; that is, we define the shift space

$$\Sigma_{\mathcal{F}} \exists\, t \in \mathbb{Z} \text{ such that } s_{t-1} = s_{t+1} = -\}\,.$$

This subshift can be easily described as a subshift on 2-blocks represented by the space $\{--, -+, +-, ++\}^{\mathbb{Z}}$, so that any point $\mathbf{s} \in \Sigma_{\mathcal{F}}$ becomes the overlapping sequence $\ldots (s_{t-1}s_t)(s_t s_{t+1}) \ldots$. The subshift on the two-block space is represented by a vertex graph with the state transition matrix

$$S = \begin{pmatrix} 0 & 0 & 1 & 0 \\ 1 & 0 & 1 & 0 \\ 0 & 0 & 0 & 1 \\ 0 & 1 & 0 & 1 \end{pmatrix}\,,$$

which indicates by 1 the allowed transitions among the four states. The number of periodic orbits of period n for the subshift is given by

$$\mathrm{Tr}(S^n) = \gamma^n + (1-\gamma)^n + 2(-1)^{n/2}(n-1 \mod 2)\,,$$

where $\gamma = (1+\sqrt{5})/2$ is the golden mean. Thus the topological entropy for $\Sigma_{\mathcal{F}}$ is $\ln\gamma$. The number of distinct periodic orbits can be obtained from this by subtracting the number of periodic orbits for all factors of n and then dividing by the number of cyclic permutations, n. For comparison with the full shift and with the numerical results below, we give a list of these in Table 2. For example there are a total of $1,465,020$ periodic points of the full shift with period $n \le 24$, while there are only $12,216$ in the subshift $\Sigma_{\mathcal{F}}$.

When b is non-negative, orbits with symbol sequences in the subspace $\Sigma_{\mathcal{F}}$, can be shown to persist longer than a general orbit:

Period	Σ	$\Sigma_{\mathcal{F}}$
1	2	1
2	1	0
3	2	1
4	3	2
5	6	2
6	9	2
7	18	4
8	30	5
9	56	8
10	99	11
11	186	18
12	335	25
13	630	40
14	1161	58
15	2182	90
16	4080	135
17	7710	210
18	14532	316
19	27594	492
20	52377	750
21	99858	1164
22	190557	1791
23	364722	2786
24	698870	4305
25	1342176	6710
26	2580795	10420
27	4971008	16264
28	9586395	25350
29	18512790	39650
30	35790267	61967

Table 2: Number of orbits with minimal period n of the 2-shift and the subshift $\Sigma_{\mathcal{F}}$.

Theorem 2 (Existence and Uniqueness of $\Sigma_{\mathcal{F}}$ orbits). *Suppose* $0 \leq b \leq 1$. *For every symbol sequence* $\mathbf{s} \in \Sigma_{\mathcal{F}}$ *there exists a unique orbit* $\mathbf{z}(\epsilon)$ *of the Hénon map Eq. (1) such that* $\mathbf{z}(0) \equiv \mathbf{s}$ *providing* $0 \leq \epsilon < \epsilon_{\max}$, *where*

$$\epsilon_{\max} \equiv \frac{2}{1+b}\sqrt{\frac{-b^2+2b+5-2\sqrt{5+4b}}{(b-1)(b-5)}}\,. \tag{12}$$

This theorem follows from the same argument that gave Thm. 1 with only minor modifications. We summarize the changes in the argument in the following discussion.

When $0 \leq b \leq 1$, $\mathbf{s} \in \Sigma_{\mathcal{F}}$, and $\mathbf{z} \in B_M$, we can bound the norm of iterates of $\mathbf{T}$ in Eq. (7) using the inequalities

$$\alpha_k \leq ||\mathbf{T}^k(z)||_\infty \leq \beta_k\,,$$

where the coefficients α_k and β_k are determined by the recursions

$$\begin{aligned} \beta_k &= \sqrt{1+\epsilon(1+b)\beta_{k-1}}\,, \\ \alpha_k &= \sqrt{1+\epsilon(b\alpha_{n-1}-\beta_{n-1})}\,, \end{aligned}$$

with $\beta_0 = 1+M$ and $\alpha_0 = 1-M$. The sequence β_k is the same as that in [6]; it has the unique attracting fixed point

$$\beta_\infty = \frac{1}{2}\left\{\epsilon(1+b)+\sqrt{\epsilon^2(1+b)^2+4}\right\}\,.$$

Since the recursion for $\{\alpha_n\}$ depends on β, but not vice versa, the coupled system also has a unique attracting fixed point, which is given by $(\alpha_\infty, \beta_\infty)$ with

$$\alpha_\infty = \frac{1}{2}\left\{\epsilon b+\sqrt{\epsilon^2 b^2+4(1-\epsilon\beta_\infty)}\right\}\,.$$

This implies that for large enough n, $\mathbf{T}^n$ maps the ball $B_{1-\alpha_\infty}$ into itself. The map $\mathbf{T}$ is a contraction map on this ball providing $||D\mathbf{T}^k||_\infty < 1$. This leads to the same bound as that in [6], namely:

$$\epsilon_{\max}(1+b) < 2\alpha_\infty\,.$$

After some simplification, this inequality yields the formula for $\epsilon_{\max}$. □

6 Horseshoe Boundary

The existence theorem 1 provides an analytical bound on the parameter range for which the Hénon map has a hyperbolic horseshoe. This bound is shown as the boundary of the dark grey region in Fig. 1. In addition Thm. 2

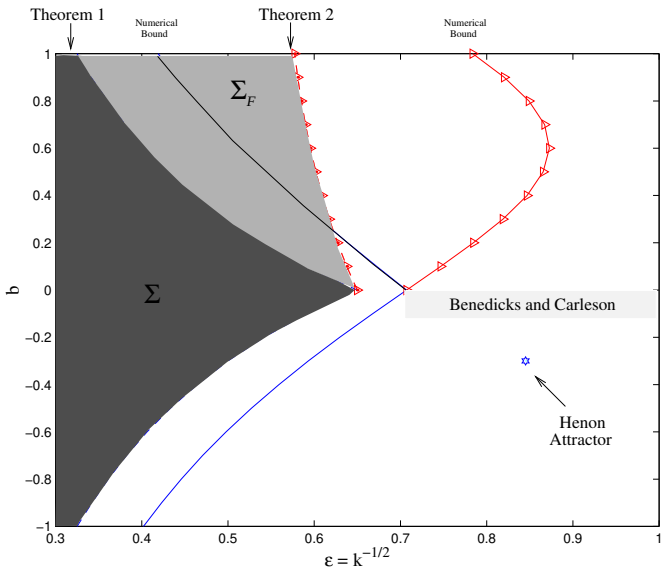

Figure 1: First bifurcations for the Hénon Map. The dark shaded region represents Thm. 1 and the lighter that of Thm. 2. The curves represent the numerical results for the first orbits destroyed up to period 24. Numerical bounds for the subshift $\Sigma_{\mathcal{F}}$ are indicated with a triangle symbol.

gives an analytical bound, shown as the boundary of the lighter shaded area in the figure, for the existence of all orbits in the subshift $\Sigma_{\mathcal{F}}$. This bound is valid only for $b \geq 0$, and meets the former at $b = 0$.

Here, we use our continuation method to estimate the boundary of existence of the horseshoe by following all orbits from the anti-integrable limit up to some fixed period, in this case period 24. In order for the numerical boundary to be valid, we must assume

Conjecture 1. *Every orbit of the Hénon map can be continuously connected to the anti-integrable limit;*

that is, there are no isolated "bubbles" in the bifurcation diagram. As far as we know, this is true for the Hénon map, but it has not been proven. Moreover, we must assume that the boundary that we compute for finitely many orbits is indeed an approximation of the boundary for all orbits. Our evidence for this is based on extrapolation, as we explain below.

To construct a numerical approximation for the boundaries, we first generate all symbol sequences for orbits of periods up to $n = 24$. Then, for fixed b, we numerically continue each orbit in ϵ away from the anti-integrable limit and monitor its multipliers to detect bifurcations. For each b we record the smallest value of ϵ at which a bifurcation occurs. The resulting numerical bound in Fig. 1 is shown as the solid curve.

The numerical bound is similar in shape to the analytical one, but shifted to the right in ϵ. While the analytical bound is symmetric under $b \to -b$,

the numerical results are not. For example the first bifurcation at $b = 1$ occurs for $\epsilon \approx 0.41888$, while at $b = -1$ it occurs for $\epsilon \approx 0.40167$. In the logistic limit ($b = 0$), Eq. (1) reduces to the logistic map,

$$z_{t+1} = \frac{1}{\epsilon}(z_t^2 - 1)\,, \tag{13}$$

for which the first bifurcation occurs at $\epsilon = 1/\sqrt{2}$, where the orbit of the critical point becomes bounded.

When b is positive, the symbol sequences for the first pair of orbits destroyed up to period 24 extrapolate to orbits that are homoclinic to the fixed point $(+)^\infty$; we conjecture that these are the first orbits destroyed as ϵ increases from 0:

Conjecture 2. *For positive b, the first bifurcation as ϵ increases from 0 corresponds to the homoclinic saddle-node bifurcation*

$$\mathrm{sn}\left\{+^\infty - (+) - +^\infty, +^\infty - (-) - +^\infty\right\}. \tag{14}$$

A theorem of Smillie [25] implies that the first bifurcation destroying the Hénon horseshoe must be a quadratic homoclinic tangency for *some* orbit. Our observations imply that it is a homoclinic bifurcation of $(+)^\infty$. When $b < 0$, however, the most natural description of the first bifurcation is as a heteroclinic tangency, which leads to

Conjecture 3. *For negative b, the first bifurcation as ϵ increases from 0 corresponds to the heteroclinic saddle-node bifurcation*

$$\mathrm{sn}\left\{-^\infty + (-) - +^\infty, -^\infty + (+) - +^\infty\right\}.$$

This does not contradict Smillie's theorem, as there are many homoclinic bifurcations that accumulate on this heteroclinic bifurcation. For example, for each m the orbits $(-^m + + - +^m)^\infty - +(-^m + + - +^m)^\infty$, are homoclinic to the periodic orbit $(-^m + + - +^m)$, and the bifurcation points of these homoclinic orbits limit on that of the heteroclinic orbits as $m \to \infty$.

Filtering the symbol sequences to choose only those in the subshift $\Sigma_{\mathcal{F}}$, we can use the same numerical data previously described to find the first bifurcation amongst the orbits in $\Sigma_{\mathcal{F}}$. This gives the solid curve marked with triangles in Fig. 1. This curve has a qualitatively different shape than the analytical bound.

For reference we indicate in Fig. 1 the point $k = 1.4$, and $b = -0.3$, corresponding to the much studied Hénon attractor. We also show the parameter range (b small enough, $1 < k < 2$) for which the theorem of Benedicks and Carleson [26] implies that the Hénon map has a transitive attractor with positive Lyapunov exponent.

7 Homoclinic Orbits

In this section we use the symbolic dynamics to classify the orbits of the Hénon map that are homoclinic to the hyperbolic fixed point $p = (+)^\infty$ and study some of the bifurcations that occur. We begin with some general terminology, referring to the Hénon map as an example.

Let f be an orientation preserving map[2] of the plane with hyperbolic fixed point p. The stable and unstable manifolds of p are denoted by W^u and W^s, and a closed segment of such a manifold between two points α and β by $W^u[\alpha, \beta]$. We use a parenthesis to denote an open endpoint of a segment. A segment that extends to the fixed point, e.g. $W^u(p, \alpha]$, is called an *initial segment* of the manifold. The set of homoclinic orbits is the set of intersections $W^s \cap W^u$. A point α is on a *primary* (or principal) homoclinic orbit if the two initial segments to α touch only at α, i.e.,

$$W^u(p, \alpha] \cap W^s(p, \alpha] = \{\alpha\}\,.$$

Thus the initial segments to a primary homoclinic orbit define a Jordan curve; we call the interior of this curve a resonance zone. More generally, a *resonance zone* is a region bounded by alternating initial segments of stable and unstable manifolds [27, 28].

For example, in Fig. 2 we sketch the left-going branches of the manifolds from $p = (+)^\infty$ for the area-preserving Hénon map. There are precisely two primary homoclinic orbits; in the figure, we label points on these orbits with α and ζ. We choose to use α to construct the resonance zone.

The stable manifold is divided into two invariant branches by the fixed point. An ordering is defined on each branch of W^s, so that $\beta <_s \gamma$ for two points on a branch of W^s if β is nearer to p along W^s than γ, i.e., $\beta \in W^s(p, \gamma)$. We similarly define an ordering $<_u$ on each branch of W^u.

A segment of a manifold from a point to its iterate, $W^s(\beta, f(\beta))$, is called a *fundamental segment* [28]. The union of the iterates of a fundamental segment is the entire branch of the manifold. Moreover, since the iterates are disjoint, every homoclinic orbit on this branch must have precisely one point on each fundamental segment.

For the Hénon map, we focus on the left-going branches of W^s and W^u and the fundamental segments between $f^{-1}(\zeta)$ and ζ. These also form the boundaries of the incoming and exit sets for the resonance zone defined by α [29]. The exterior halves of these segments, $W^s(\alpha, \zeta)$ and $W^u(f^{-1}(\zeta), \alpha)$, contain no homoclinic points since orbits on these segments are unbounded, so it is sufficient to look for homoclinic points on the interior halves,

$$\begin{aligned} U &\equiv W^u[\alpha, \zeta]\,, \\ S &\equiv W^s[f^{-1}(\zeta), \alpha]\,. \end{aligned} \tag{15}$$

[2]The orientation reversing case could be included by considering f^2, since its manifolds have the same geometry as those of f.

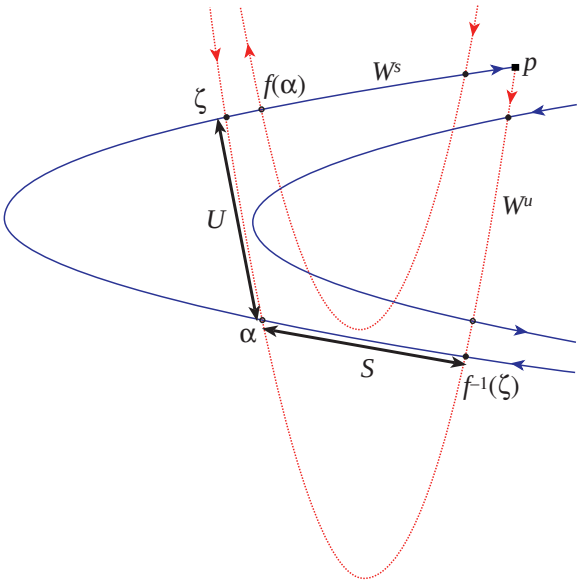

Figure 2: Stable and unstable manifolds for the Hénon map at $k = 5$ and $b = 1$ shown in (z, z') coordinates.

Every homoclinic orbit must have exactly one point on both S and U.

Homoclinic orbits can be classified in a number of ways. The *type* [28], of a homoclinic point β is[3]

$$\text{type}(\beta) = \sup\{j \geq 0 : W^s(p, f^j(\beta)] \cap W^u(p, \beta] \neq \emptyset\}\,;$$

i.e., the number of iterates for which the stable initial segment to $f^j(\beta)$ intersects with the unstable initial segment to β. The type of a homoclinic point is invariant along its orbit. Primary homoclinic points have type 0.

Homoclinic orbits on particular branches of W^s and W^u can also be classified by their *transition time*. In general this is defined relative to a choice of a primary homoclinic point, ζ and the fundamental segments $W^u(f^{-1}(\zeta), \zeta]$ and $W^s(f^{-1}(\zeta), \zeta]$. Any homoclinic orbit on these branches has exactly one point, β, on the unstable segment. The transition time is the number of iterates required for $\beta \in W^u(f^{-1}(\zeta), \zeta]$ to reach the stable segment:

$$t_{\text{trans}}(\beta) = k \text{ if } f^k(\beta) \in W^s(f^{-1}(\zeta), \zeta]$$

The value of the transition time depends upon the choice of fundamental segments, so it is not as basic a property as the type.

In the simplest case, the transition time is easily related to the type of the orbit [1]:

[3]Our definition of the type differs from Easton's slightly, to comply with his definition that type 1 is equivalent to the horseshoe. Rom-Kedar [30] uses the term *Birkhoff signature* instead of type.

Lemma 3. *Assume there are exactly two primary homoclinic orbits, ζ and α, and the segments S and U defined as Eq. (15) contain all of the homoclinic orbits. Then for each homoclinic point in $\beta \in U$, $t_{\rm trans}(\beta) = {\rm type}(\beta)$.*

Proof: If $\beta \in U$ is of type t, then by definition $W^s(p, f^t(\beta)] \cap W^u(p, \beta] \neq \emptyset$. Now since $\alpha <_u \beta <_u \zeta$ and $W^s(p,\zeta) \cap W^u(p,\zeta) = \emptyset$, this implies that $\alpha <_s f^t(\beta)$. However, $W^s(p, f^{t+1}(\beta)] \cap W^u(p,\beta] = \emptyset$, which means that $f^{t+1}(\beta) <_s \alpha$, but there are no homoclinic points on $W^s(\zeta,\alpha)$, so actually $f^{t+1}(\beta) <_s \zeta$. Now S contains every homoclinic point that reaches $W^s(p,\zeta)$ in one iteration, so $f^t(\beta) \in S$. □

Each homoclinic orbit has a Poincaré signature that determines the direction of crossing of W^u and W^s at points on the orbit. We define the signature to be $+1$ if, looking along the unstable manifold in the direction of motion, the stable manifold crosses the unstable from the left to the right side. Crossings in the opposite direction have signature -1. If the manifolds do not cross but only touch (a topologically even intersection), the signature is defined to be zero. Since the map is orientation preserving, the signature is invariant along an orbit. Thus in Fig. 2 α and ζ have signatures -1 and $+1$, respectively. The signature of a particular homoclinic orbit is typically not preserved in a bifurcation, but the total signature of the bifurcating orbits must be the same on each side of the bifurcation value. For example a saddle-node bifurcation creates a zero signature orbit that splits into one positive and one negative signature orbit.

For the Hénon map, the AI symbol sequence leads to a complete classification of homoclinic orbits. It is easy to construct homoclinic and heteroclinic orbits using the symbolic dynamics: an orbit heteroclinic from a periodic orbit $(s)^\infty$ to a periodic orbit $(s')^\infty$ has a symbol sequence that begins with a head sequence $(s)^\infty$ and ends with a tail sequence $(s')^\infty$ with some arbitrary, finite symbol sequence separating the head and tail. For example, the simplest orbits homoclinic to $p = (+)^\infty$ are the primary homoclinic orbits:

$$\begin{aligned} \zeta &= +^\infty - \,.\, +^\infty , \\ \alpha &= +^\infty - \,.\, - +^\infty , \end{aligned} \tag{16}$$

corresponding to those we labeled in Fig. 2. These symbol sequences arise because as $\epsilon \to 0$ the point α moves to the point $-\,.\,-$, while ζ moves to $-\,.\,+$ and $f^{-1}(\zeta)$ to $+\,.\,-$.

All other orbits homoclinic to p can be written in the form $+^\infty - (s) - +^\infty$, where s, the *core*, is any finite sequence—thus there is a one-to-one correspondence between finite symbol sequences and potential homoclinic orbits (all of which exist in the AI limit). This implies, for example, that near the anti-integrable limit there are 2^k homoclinic orbits with core length k. We will often denote a homoclinic orbit simply by writing the core, (s).

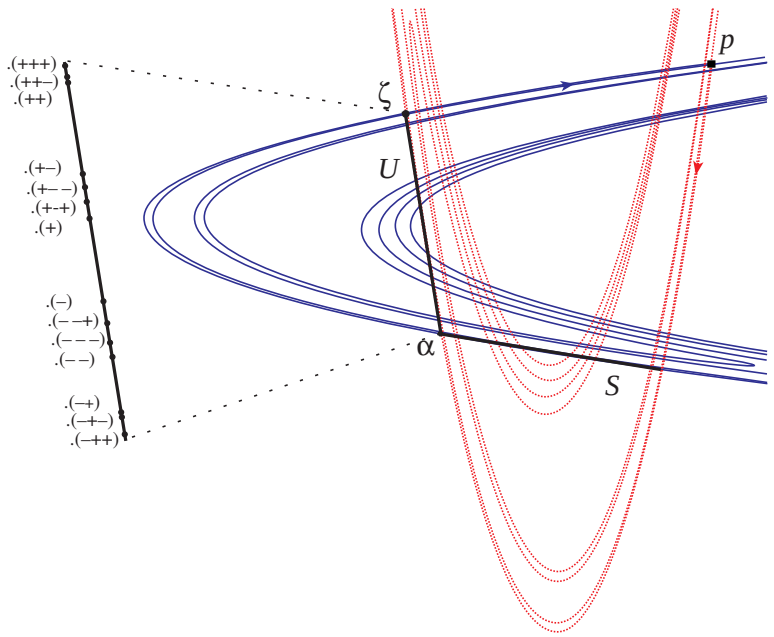

Figure 3: Ordering of homoclinic orbits of type 3 or less at $k = 6.25$. The enlargement on the left shows the core sequences for the 14 homoclinic orbits.

The classification of homoclinic orbits by their symbol sequence can be used to compute other invariants. To determine the type of an orbit, we simply note that the AI symbols give exactly the same coding for an orbit as the standard symbolic coding for the horseshoe. This implies that the point $+^\infty - \mathbf{.}(s) - +^\infty$ corresponds to a phase point on U, and the point $+^\infty - (s)\mathbf{.} - +^\infty$ is on S, thus

Lemma 4. *The transition time of the homoclinic orbit close to the AI limit is given by the length of the core sequence.*

For example, the homoclinic orbit $+^\infty - (- - +) - +^\infty$ has the core sequence $(- - +)$, and therefore has transition time 3.

Similarly the signature of a homoclinic orbit in the horseshoe is given by simply counting the number of $-$ signs in the core sequence.

Lemma 5. *The signature of a homoclinic orbit with core (s) close to the AI limit is given by $-(-1)^j$ where j is the number of $-$ signs in s.*

Thus the orbit $(- - +)$ has signature -1.[4] We will see that, when $b = 1$, some homoclinic orbits undergo pitchfork bifurcations, which change their signature, so this rule is not valid for all parameter values.

The positions of the homoclinic orbits on U for orbits of type 1, 2 and 3, labeled by their core sequences, are shown in Fig. 3. The order of the

[4]Eq. (11) implies that the signature is the same as the limiting sign of the residue of periodic orbits that approximate the homoclinic orbit.

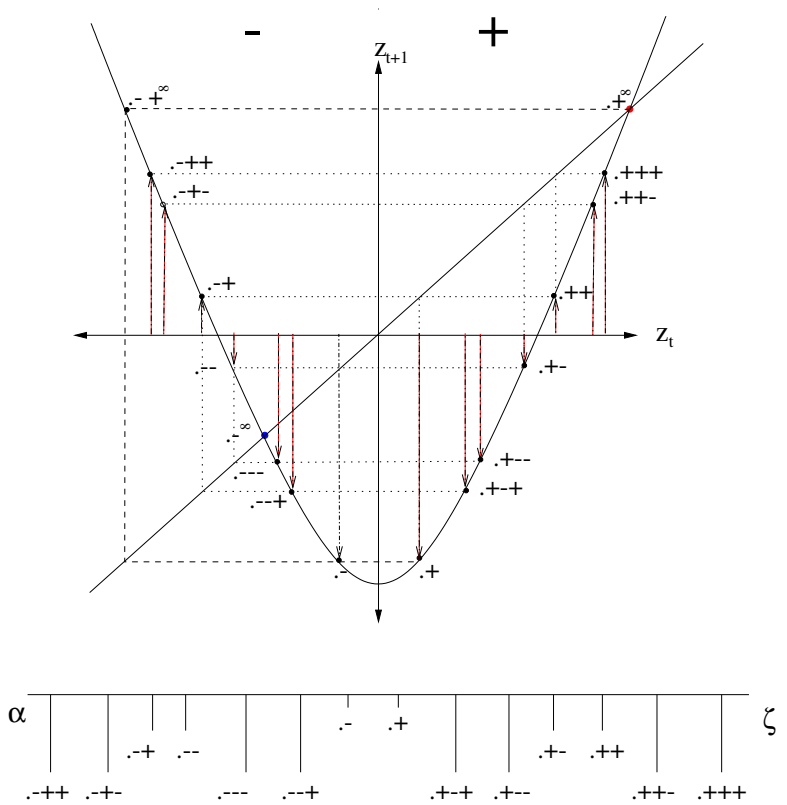

Figure 4: Ordering of pre-periodic points for the + fixed point of the logistic limit of the Hénon map. The symbols are determined by the itinerary of the orbit relative to the critical point at $z = 0$.

homoclinic orbits on the segments S and U, when they exist, must be the same as the corresponding ordering of homoclinic points in the complete horseshoe, since they cannot collide except when there is a bifurcation, and we observe that every such collision destroys homoclinic orbits moving away from the AI limit. This ordering is equivalent to that of the logistic map, Eq. (13), for the orbits forward asymptotic to the + fixed point. This gives an easy way to compute the ordering, see Fig. 4. In the logistic limit, all of the sequences forward asymptotic to the fixed point are destroyed when the orbit of the critical point becomes bounded at $\epsilon = 1/\sqrt{2}$. The fixed point $.+^\infty$ has a single preimage, which is $\alpha = .-+^\infty$. Every other orbit that is forward asymptotic to $.+^\infty$ has the form $.(s)-+^\infty$.

The ordering of the orbits along S is equivalent to that on U upon time reversal. Thus a type t point $+^\infty - (s_1 s_2 \dots s_t).-+^\infty$ on S is in the same relative position as the point $+^\infty - .(s_t s_{t-1} \dots s_1) - +^\infty$ on U.

So long as there are no homoclinic bifurcations, then the orderings $>_u$ and $>_s$ are just given by the usual unimodal ordering as stated in

Lemma 6. *The ordering $>_u$ on U and $>_s$ on S close to the AI limit is*

given by

$$\begin{array}{llll} +^\infty - \bullet e + \ldots & >_u & +^\infty - \bullet e - \ldots \\ +^\infty - \bullet o + \ldots & <_u & +^\infty - \bullet o - \ldots \\ \cdots + e \bullet - +^\infty & >_s & \cdots - e \bullet - +^\infty \\ \cdots + o \bullet - +^\infty & <_s & \cdots - o \bullet - +^\infty \,, \end{array}$$

where e / o are finite sequences with an even / odd number of minus signs, respectively.

The ordering shown in Fig. 3 and Fig. 4 is exactly this one upon appending the "homoclinic tail" $-+^\infty$ to the cores. The maximal orbit on U is ζ, corresponding to the tail $\bullet+^\infty$, the minimal orbit is α, corresponding to $\bullet - +^\infty$.

8 Homoclinic Bifurcations

Homoclinic bifurcations are bifurcations between homoclinic orbits. Compared to ordinary bifurcations of periodic orbits they possess additional structure because the invariant manifolds (with their ordering) must be involved in the bifurcation process. Two homoclinic orbits β and γ are *double neighbors* if the segments $W^u[\beta,\gamma]$ and $W^s[\beta,\gamma]$ contain no other homoclinic orbits. Three ordered homoclinic points $\beta <_u \gamma <_u \delta$ are *triple neighbors* if both β,γ and γ,δ are double neighbors. An obvious observation with nevertheless important consequences is the "double neighbor" lemma:

Lemma 7. *Two homoclinic orbits β and γ cannot bifurcate unless they are double neighbors.*

The converse gives a simple forcing relation: before β and γ can bifurcate any homoclinic orbit on either segment between them must have disappeared.

Another consequence is the transition time lemma:

Lemma 8. *If two homoclinic orbits β and γ bifurcate then they must have the same transition time $t_{\rm trans}$.*

Proof: Let β and γ be neighbors on U. If their transition time is different then they are not neighbors on S, so they cannot bifurcate. □

This allows us to extend Lemma 4 away from the AI limit, so that one can take the transition time as an adequate replacement of the period:

Corollary 9. *The transition time of a homoclinic orbit never changes.*

Proof: Since the transition time is an integer it cannot change under smooth deformations. It could only change at bifurcations, but we have just seen that only orbits with the same transition time bifurcate. □

Therefore bifurcations only take place between double neighbors with the same transition time, i.e. core length. In order to determine which orbits are neighbors we make the assumption that the following symbolic ordering conjecture holds:

Conjecture 4. *The symbolic horseshoe ordering on the invariant manifolds given in Lemma 6 persists.*

Close to the AI limit the horseshoe is still complete. In this situation it is possible to find all neighbors:

Lemma 10. *Two homoclinic orbits on U are neighbors in the complete horseshoe if and only if they are of the form $+^\infty - \bullet(s+) - +^\infty$ and $+^\infty - \bullet(s-) - +^\infty$.*

Proof: We have to show that there is no homoclinic orbit with core δ such that $(o+) <_u (\delta) <_u (o-)$ or $(e-) <_u (\delta) <_u (e+)$, where $e = s$ if s has an even number of minus signs or $o = s$ if this number is odd. If the initial string in δ differs from s then δ can not be between the sequences $(s-)$ and $(s+)$, therefore $\delta = s\ldots$. It is simple to see that

$$\bullet e + \cdots \geq_u \bullet e + -+^\infty, \quad \bullet e - \cdots \leq_u \bullet e - -+^\infty,$$

and similarly

$$\bullet o + \cdots \leq_u \bullet o + -+^\infty, \quad \bullet o - \cdots \geq_u \bullet o - - +^\infty .$$

Since $\delta = s\ldots$ it must be of one of the forms on the left hand sides, but then the inequalities show that it is not between $(s+)$ and $(s-)$ hence they must be neighbors. Conversely, suppose we have two neighboring homoclinc orbits (on U) $\bullet a$ and $\bullet b$ with $\bullet a <_u \bullet b$. They must differ in at least one symbol so call the first such difference x. Their leading common symbols are denoted by s, so that $a = sx\alpha$ and $b = s\bar{x}\beta$ for some sequences α and β. Applying the ordering relation to the possible combinations of s and x gives either

$$\bullet e - \alpha <_u \bullet(ey) - +^\infty <_u \bullet e + \beta \quad \text{or} \quad \bullet o + \alpha <_u \bullet(oy) - +^\infty <_u \bullet o - \beta,$$

where the choice of the symbol y depends on whether s is even or odd and whether α and β are $-+^\infty$. Specifically, choose $y = +$ if either $s = e$ and $\beta \neq -+^\infty$ or $s = o$ and $\alpha \neq -+^\infty$. Choose $y = -$ if either $s = e$ and $\alpha \neq -+^\infty$ or $s = o$ and $\beta \neq -+^\infty$. If neither α nor β are $-+^\infty$ either choice

for y works. When either α,β, or both differ from $-+^\infty$ we've constructed an orbit

$$.\delta \equiv .(sy) - +^\infty$$

which is between $.a$ and $.b$—hence $.a$ and $.b$ are *not* neighbors. But this is a contradiction so $\alpha, \quad \beta = -+^\infty$. □

For a bifurcation to occur it is not enough that the orbits be neighbors on U, but they must be double neighbors. This almost gives the proof of Conjecture 2, but here we're working in the smaller class of orbits homoclinic to p, the hyperbolic fixed point. Note that the following theorem does not rely on the symbolic ordering conjecture, because the ordering is used in a range of parameters before the first bifurcation occurs, so the horseshoe ordering is still valid.

Theorem 11. *The first homoclinic bifurcation of the invariant manifolds of the fixed point* $(+)^\infty$ *is*

$$\mathrm{sn}\left\{+^\infty - (+) - +^\infty, +^\infty - (-) - +^\infty\right\}.$$

Proof: By Lemma 10 we know that all neighbors on U in the complete horseshoe are of the form $(s\pm)$. For them to be double neighbors, these sequences must be neighbors on S as well, but this is equivalent to the sequence and reverse being neighbors on U. But this only true if s is empty. The only double neighbors in the complete horseshoe are therefore the two orbits $+^\infty - (+) - +^\infty$ and $+^\infty - (-) - +^\infty$. Therefore they must bifurcate first. □

To approximate a homoclinic orbit, which possesses an infinite number of points in phase space with a periodic orbit with only a finite number of points we require that the Hausdorff distance of these two point sets vanishes in the limit of infinite period. Thus for an orbit homoclinic to $(+)^\infty$, we study a sequence of approximating periodic orbits with an increasingly long string of + symbols. In particular the rotational orbits given in Eq. (9) converge to ζ and α in the limit.

In Table 3 we list the first 11 members of the sequence approximating the transit time 1 homoclinic orbit, and the corresponding sequence of values, ϵ_{sn} at which these orbits undergo a saddle-node bifurcation when $b = 1$. These values converge geometrically to the parameter at which the homoclinic orbits bifurcate, and the ratio of successive differences (a "Feigenbaum ratio") is computed in the fourth column of the table. As is known theoretically, the convergence rate, δ, approaches λ, the multiplier of the fixed point, p

Orbits	$\epsilon_{\rm sn}$	ϵ_∞	δ
$(-*-+^2)^\infty$	0.4244113099817847	0.418886386005370	
$(-*-+^3)^\infty$	0.4196139686609910	0.418879425211360	7.03462660
$(-*-+^4)^\infty$	0.4189824163820134	0.418879238282474	7.03430596
$(-*-+^5)^\infty$	0.4188938699141631	0.418879233464361	7.03442728
$(-*-+^6)^\infty$	0.4188813132707083	0.418879233345500	7.03444522
$(-*-+^7)^\infty$	0.4188795290018318	0.418879233342659	7.03444521
$(-*-+^8)^\infty$	0.4188792753723665	0.418879233342592	7.03445672
$(-*-+^9)^\infty$	0.4188792393174328	0.418879233342592	7.03445932
$(-*-+^{10})^\infty$	0.4188792341919594	0.418879233342590	7.03444699
$(-*-+^{11})^\infty$	0.4188792334633355	0.418879233342590	7.03443417
$(-*-+^{12})^\infty$	0.4188792333597558	0.418879233342592	
$(-*-+^{13})^\infty$	0.4188792333450313	0.418879233342590	
$(-*-+^{14})^\infty$	0.4188792333429387		
$(-*-+^{15})^\infty$	0.4188792333426405		

Table 3: Bifurcations in periodic approximations to the homoclinic transit time 1 orbit, which is the first orbit destroyed. Here we use a $*$ to denote both $+$ and $-$, giving both orbits involved in the bifurcation.

[31, 15][5]. Our observations verify this to six digits, since

$$\lambda \approx 7.0344478$$

for the fixed point p when $\epsilon \approx 0.41887923$. The third column in the table is the extrapolation for the converged ϵ value, given by Aitken's Δ^2 method

$$\epsilon_\infty = \epsilon_n - \frac{\Delta(\epsilon_{n+1})^2}{\Delta^2(\epsilon_{n+2})}\,,$$

where Δ is the standard discrete difference operator. Thus we see that there is a saddle-node bifurcation of the type 1 homoclinic orbits,

$$\mathrm{sn}\left\{+^\infty-(+)-+^\infty, +^\infty-(-)-+^\infty\right\},$$

at

$$\epsilon_{\rm sn}(1) \approx 0.41887923334259 \quad \text{or} \quad k_{\rm sn}(1) \approx 5.699310787383\,.$$

This also corresponds to the parameter value at which the topological horseshoe for the Hénon map is destroyed, and is the value in Fig. 1 at $b = 1$.

Since there is a sequence of saddle-node bifurcations that limit on the homoclinic bifurcation, there are elliptic islands arbitrarily close to the destruction of the horseshoe. This is a simple illustration of the theorems

[5] Although Robinson proved this result for the dissipative case, the result should hold as well for the area preserving case

proved by Newhouse [32, 12], and corresponds to an area-preserving version of the results of Gavrilov and Silnikov [13, 14].

Since we can in principle follow every finite orbit from the anti-integrable limit we can begin to study the sequence of bifurcations that occur after the horseshoe is destroyed, see Table 4. For example, the bifurcation diagram for all of the homoclinic orbits of type three or less is sketched in Fig. 5. The vertical ordering in this sketch is the same as that on the segment U with α and ζ shown. The bifurcation diagram is highly influenced by the time-reversal symmetry of the area-preserving Hénon map—we will discuss this symmetry in the next section. As expected from the general theory [33], we observe three kinds of bifurcations:

Symmetric saddle-node bifurcations resulting in the creation of a pair of type t homoclinic orbits with opposite signatures. For example, in Fig. 5, the type 3 orbits with cores $(+++)$ and $(-+-)$ are born in such a saddle-node at $k \approx 0.386$.

Pitchfork bifurcations of a type t symmetric homoclinic orbit, creating a pair of type t asymmetric orbits that are related by time reversal. For example, the $(-+-)$ orbit pitchforks at $k \approx 0.720$ creating the orbits $(-++)$ and $(++-)$. A pitchfork bifurcation requires triple neighbors to occur.

Asymmetric saddle-node bifurcation creating two symmetry related pairs of asymmetric orbits. This bifurcation first occurs at type 4. For example the two pairs $\{(-+--), (-+-+)\}$ and $\{(--+-), (+-+-)\}$ are created at $k \approx 5.18$. Generically, asymmetric saddle-node bifurcations require two pairs of double neighbors to occur because of the symmetry.

The shaded region in Fig. 5 represents the range of k for which the area preserving Hénon map exhibits a horseshoe. Along the left edge we label each orbit with its core symbol sequence.

The first type t homoclinic orbits are created by a saddle-node bifurcation when the segment $f^{-t}(S)$ first intersects U. We denote this parameter value by $k_{\rm sn}(t)$. This marks the creation of the subset of the incoming lobe of the turnstile with transit time t [29]. We observe that when $b = 1$, this homoclinic saddle-node bifurcation is

$$\mathrm{sn}\,\{(+^t), (-+^{t-2}-)\}\,, \quad \text{occurring} \quad \mathrm{at} k_{\rm sn}(t)\,.$$

Following this, the orbit $(-+^{t-2}-)$ undergoes a homoclinic pitchfork bifurcation at $k_{\rm pf}(t)$, creating the pair

$$(-+^{t-2}-) \to \mathrm{pf}\,\{(+^{t-1}-), (-+^{t-1})\} \quad \text{at } k_{\rm pf}(t)\,.$$

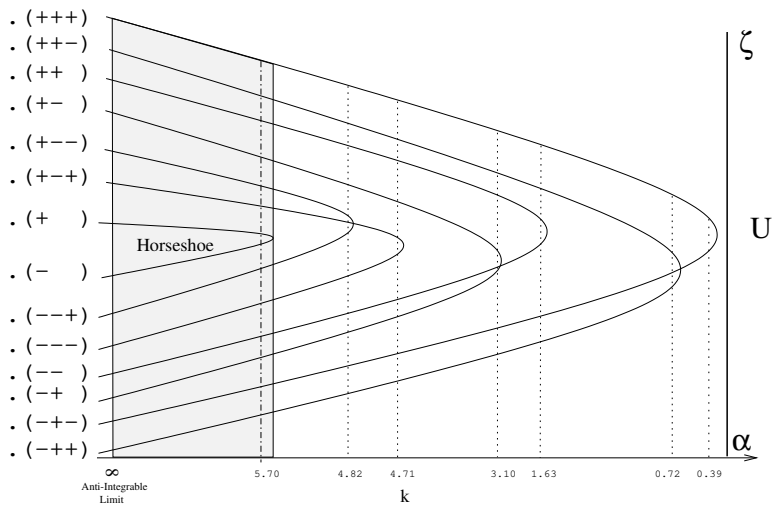

Figure 5: Sketch of bifurcations in the homoclinic orbits up to type 3 ($b = 1$).

Parent	Type	Child	Child	k-Value
	sn	$(-++-)$	$(+++)$	-0.133474
$(-++-)$	pf	$(-++)$	$(+++-)$	-0.044273
	sn	$(-+-)$	$(+++)$	0.385556
$(-+-)$	pf	$(-++)$	$(++-)$	0.719630
	sn	$(--)$	$(++)$	1.627779
$(--)$	pf	$(-+)$	$(+-)$	3.091505
	sn	$(+---+)$	$(----)$	3.98213640
$(----)$	pf	$(----+)$	$(+---)$	3.98213641
	sn	$(+-+)$	$(---)$	4.706399
$(+-+)$	pf	$(--+)$	$(+--)$	4.816792
	asn	$(-+-*)$	$(*-+-)$	5.188561
	asn	$(*-++)$	$(++-*)$	5.619922
	sn	$(+)$	$(-)$	5.699311

Table 4: Homoclinic bifurcations up to core length 4.

However, when $b \neq 1$, the initial symmetric bifurcation and the following symmetry breaking pitchfork are replaced by a pair of nonsymmetric saddle-node bifurcations. In this case the first type t bifurcation is the homoclinic saddle-node

$$\text{sn}\left\{(+^t), (+^{t-1}-)\right\}.$$

According to the double neighbor lemma, certain bifurcations cannot occur prior to other homoclinic bifurcations. The ordering relations give a unique construction of the order of the points on U and S, and this implies that a schematic construction of the intersections of $f^{-t}(S)$ with U can be constructed solely from a list of which orbits exist at a given parameter value. Such a schematic manifold plot is shown in Fig. 6, for all homoclinic orbits that exist at $k = 5.53$ up to type 5.

We can also construct a schematic bifurcation diagram for homoclinic orbits, as in Fig. 7, by drawing a horizontal line from $k = \infty$ to the k-value at which a particular homoclinic orbit is destroyed—actually we stop the figure at $k = 6$, since there are no bifurcations for larger k-values. We order the homoclinic orbits vertically according to their unimodal ordering on U as usual. In this bifurcation diagram the vertical connections indicate which orbits eventually do become neighbors and bifurcate. So as to avoid artificially crossing lines, we connect pairs of asymmetric saddle-nodes by lines at the right edge of the figure to indicate that they must bifurcate at the same k-value.

We say that a bifurcation *straddles* the centerline if the pair of orbits involved are on either side of center of the U ordering, or if one of the two pairs of an asymmetric saddle-node straddles the center line.

Through type 6, each symmetric saddle node is followed by a pitchfork bifurcation, just as we observed in Fig. 5, with the exception of the very first bifurcation, $\text{sn}\{(+), (-)\}$, which corresponds to the smallest loop straddling the center in the figure.

Moreover, it is remarkable, but perhaps misleading, that through type 6 every bifurcation straddles the center. Therefore all homoclinic bifurcations up to type 6 are forced by nesting around the center. In particular this means that their unimodal ordering gives the bifurcation ordering, like in unimodal maps.

This simple forcing relation is destroyed with the appearance of a symmetric saddle-node without pitchfork of type 7. Also at type 7, there is an asymmetric saddle-node quadruple which does not straddle the center. Interestingly enough, this is the same bifurcation that marks the upper k endpoint of the gap that we discuss in §10.

It is difficult to visualize the full homoclinic bifurcation diagram for larger type orbits. To do so, we plot only the horizontal lines, to indicate the range of existence of an orbit; such a diagram up to transition time 11 is given in Fig. 8. The approximate self-similarity in this picture seems to be related to some of the gaps we discuss in §10, namely those that are related

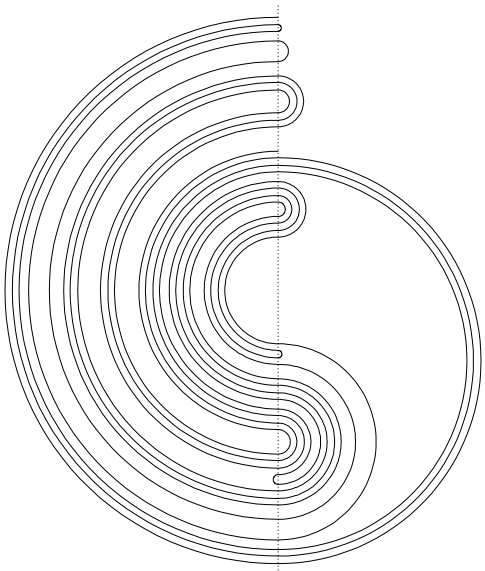

Figure 6: Schematic drawing of U and $f^{-t}(S)$ up to type 5 for $k = 5.53$.

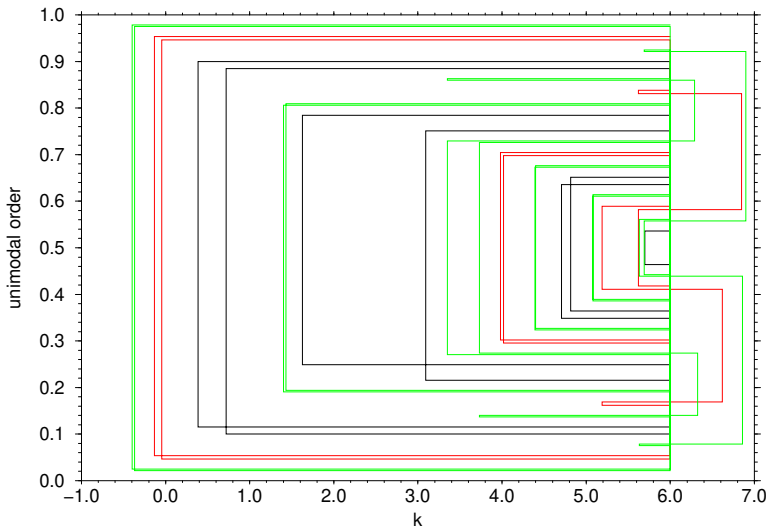

Figure 7: Bifurcation diagram of homoclinic orbits up to type 5 ($b = 1$).

to symmetric saddle-nodes without accompanying pitchforks of type 7, 9 and 11.

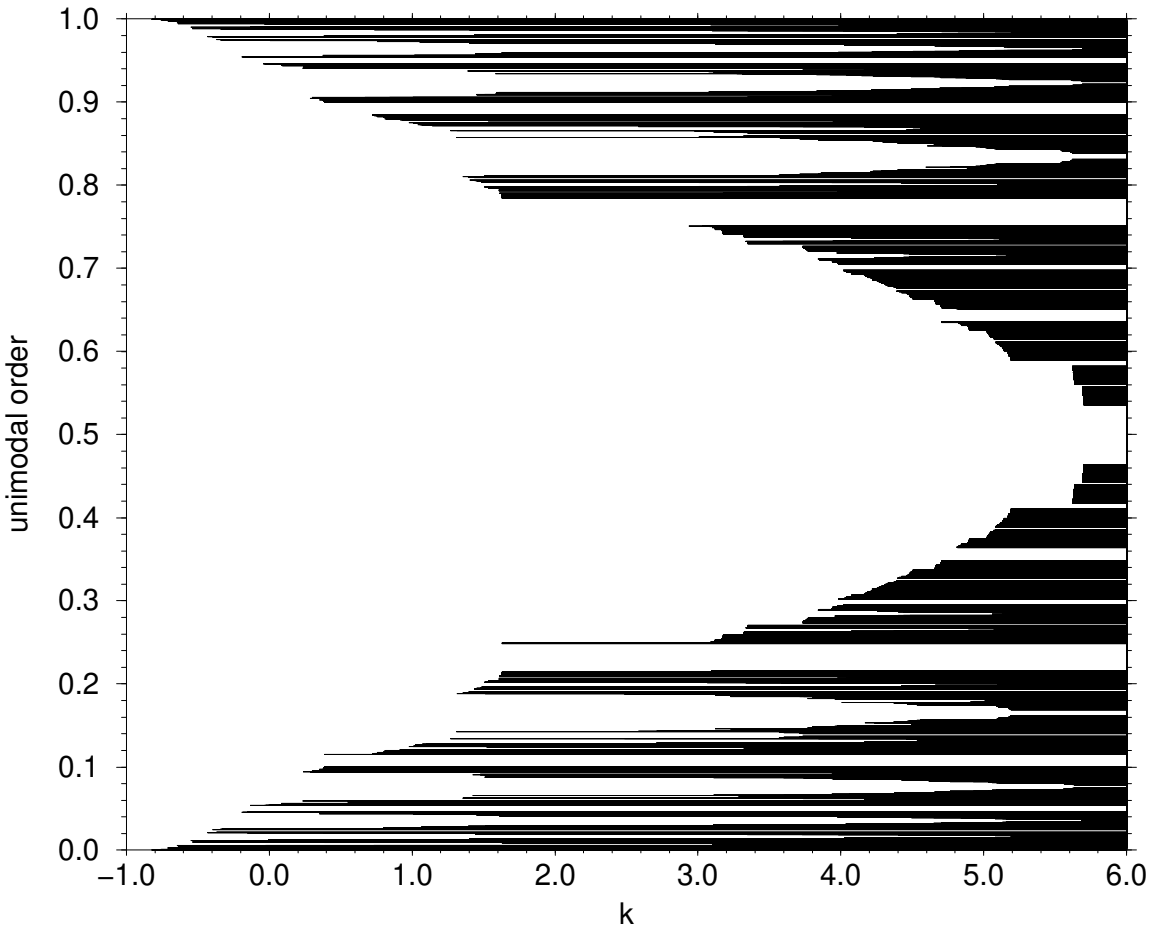

Figure 8: Existence plot of homoclinic orbits up to type 11. For each homoclinic orbit a line is drawn from large k to the parameter value where this orbit is destroyed. The vertical position of each line is its formal position on U according to the unimodal ordering.

9 Symmetric homoclinic bifurcations

As we mentioned above, the bifurcation diagram of the area-preserving Hénon map is restricted by the fact that the map has a time-reversal symmetry. Here we briefly recall a few well known facts about reversible maps [34], and apply them to the study of homoclinic bifurcations.

A map f has a time-reversal symmetry when it is diffeomorphic to its inverse by:

$$Rf = f^{-1}R\,.$$

We call the conjugacy R a reversor for f. Often, as in our case, the reversor is an involution, $R^2 = I$. Note that each of the maps f^tR is also a reversor, in particular, we call fR the complementary reversor to R. The fixed set of a reversor

$$\mathrm{fix}(R) = \{x : Rx = x\}\,,$$

are of particular interest. For the case when R is an orientation reversing involution of the plane, then $\mathrm{fix}(R)$ is always a curve that goes through infinity, thus dividing the plane into two pieces [35].

A reversor maps an orbit $\ldots z_{t-1}, z_t, z_{t+1} \ldots$ of the map onto another orbit $\ldots Rz_{t+1}, Rz_t, Rz_{t-1} \ldots$. A symmetric orbit is defined as one that is mapped onto itself by R. It is easy to see that any symmetric orbit must have points on $\mathrm{fix}(R) \cup \mathrm{fix}(fR)$. Moreover if the orbit is not periodic, it has a unique point on one of these fixed sets, and if it is periodic it has exactly two points on the fixed sets [36].

Reversible maps need not be area preserving, though the multipliers of an orbit and its symmetric pair must be reciprocals of one another. In particular, the product of the multipliers of a symmetric orbit must be one. This implies that the Hénon map is reversible only when $b = \pm 1$. For the case $b = 1$ a reversor is $R(x, y) = (-y, -x)$, and a complementary reversor $fR(x, y) = (-x - k + y^2, y)$. The fixed curves are

$$\begin{aligned} \mathrm{fix}(R) &= \{(x, y) : x = -y\}\,, \\ \mathrm{fix}(fR) &= \{(x, y) : x = \frac{1}{2}(y^2 - k)\}\,. \end{aligned}$$

Suppose that p is a symmetric, hyperbolic fixed point of a reversible map. Then, as pointed out by Devaney [37], the stable and unstable manifolds of the map are related by R:

Lemma 12. *Let W^u and W^s be the stable and unstable manifolds of a symmetric fixed point p. Then $RW^u(p, \alpha] = W^s(p, R\alpha]$.*

Proof: By definition, when $\alpha \in W^u$, then $f^{-t}(\alpha) \to p$ as $t \to \infty$. Then $Rf^{-t}(\alpha) = f^t(R\alpha) \to Rp = p$. Thus, $R\alpha \in W^s$. Since R is a diffeomorphism, $RW^u(p, \alpha] = W^s(p, R\alpha]$. □

Corollary 13. *If W^u intersects the fixed set of a reversor, then the intersection point is homoclinic.*

Homoclinic orbits of symmetric periodic orbits come in symmetric pairs, and there must exist symmetric homoclinic orbits:

Lemma 14. *Let p be a symmetric, hyperbolic fixed point, and α a homoclinic point, and suppose that R is an orientation reversing involution. Then $R\alpha$ is also a homoclinic point. Moreover, there exist symmetric homoclinic points on* $\mathrm{fix}(R)$ *and* $\mathrm{fix}(fR)$.

Proof: By Lemma 12, since $\alpha \in W^s \cap W^u$ then $R\alpha \in W^u \cap W^s$, so it is homoclinic as well. Since $\mathrm{fix}(R)$ divides the plane and α and $R\alpha$ are on opposite sides of this curve, the segment $W^u[\alpha, R\alpha]$ must cross $\mathrm{fix}(R)$, and the crossing point is necessarily homoclinic. We can argue similarly for fR. □

As is well known, pitchfork bifurcations occur with codimension one in maps with a symmetry [33]. This occurs for homoclinic bifurcations as well, as was suggested in [38]. We observed such pitchfork bifurcations in Fig. 5. A pitchfork typically occurs after a symmetric, type $t > 1$, saddle-node bifurcation creates a "tip" of W^s inside the entry lobe of the turnstile. As this tip grows, one would normally expect it to bend around, as sketched in Fig. 9, creating more type t homoclinic points by saddle-node bifurcation. In fact, it is a simple consequence of the linear ordering along W^u and W^s that a single saddle-node bifurcation like that sketched in Fig. 9 is impossible:

Theorem 15. *Suppose that f is an orientation preserving, reversible map, with a symmetric fixed point p, and S and $U = RS$ are segments of its stable and unstable manifold bounded by adjacent primary homoclinic orbits. Suppose that a pair of symmetric homoclinic points on U, $\beta <_s \gamma$ are created in a saddle-node bifurcation. Then it is impossible for there to be a single saddle-node bifurcation as a tangency of $W^s(\beta, \gamma)$ with either piece of $U \setminus W^u[\beta, \gamma]$.*

Proof: Since $\beta <_s \gamma$, and $RW^s = W^u$, we have $R\beta <_u R\gamma$. Suppose that β and γ have transition time t. Then $f^t(\beta) \in S$, but since β is symmetric this point must be the same as $R\beta$. Thus $f^{-t}(R\beta) = \beta$, and similarly for γ. Since the ordering is preserved by iteration, then $\beta <_u \gamma$. Now suppose there is a tangency at a point $\delta = W^s(\beta, \gamma) \cap (U \setminus W^u[\beta, \gamma])$, i.e. not between β and γ. We sketch such a configuration in Fig. 9. Thus $\beta <_s \delta <_s \gamma$. By symmetry, $R\beta <_u R\delta <_u R\gamma$. Since the ordering is preserved by iteration, we have $\beta <_u f^{-t}(R\delta) <_u \gamma$. Thus $f^{-t}(R\delta) \in W^u(\beta, \gamma)$ and so this point is not δ (consequently the orbit of δ is not symmetric). Since the manifolds are tangent at δ, they are also tangent at $R\delta$ by symmetry. Thus there is a second, simultaneous tangency, on U at $f^{-t}(R\delta)$ which contradicts the assumption that a single tangency occurs. □

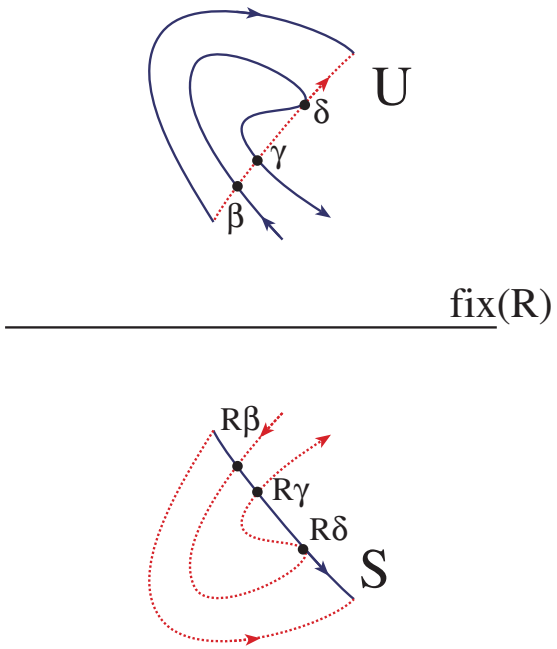

Figure 9: Impossibility of the second symmetric bifurcation as described in Thm. 15. Stable manifolds are shown as solid and unstable manifolds as dashed curves. Reflection of a tangency at δ gives a tangency at $R\delta$ that is ordered incorrectly.

There are three possible resolutions: first one of the two orbits, β or γ could undergo a pitchfork bifurcation creating a symmetry related pair of homoclinic orbits. For example, Fig. 10, shows part of the homoclinic tangle at a parameter value where the type two homoclinic orbit with core sequence $(--)$ pitchforks. As k increases this results in the creation of a pair of type 2 orbits with cores $(-+)$ and $(+-)$, see Fig. 11. Note that the new orbits are not symmetric, but that the reversal of $(-+)$ is $(+-)$, so they form a symmetric pair.

The second possible bifurcation is a single-saddle node on the segment $W^u(\beta,\gamma)$; this happens, for example, whenever a "tip" of an iterate of S returns to U. This first occurs at type 3, for the bifurcation $\mathrm{sn}\{(*-*)\}$. We sketch a similar case, at type 4, $\mathrm{sn}\{(*--*)\}$, in Fig. 12.

The third possible bifurcation is a pair of asymmetric saddle-node bifurcations. This first occurs for homoclinic orbits of type 4. For example, the bifurcations $\mathrm{sn}\{(+--+-),(---+-)\}$ and its time-reverse, $\mathrm{sn}\{(-++-+),(-+++-)\}$ occur at $k = 5.1885$. We sketch U and $f^{-4}(S)$ at this bifurcation in Fig. 12. This bifurcation also corresponds to the lower endpoint of an apparently hyperbolic parameter interval for the Hénon map, as we discuss in the next section.

A symmetric saddle-node followed by a pitchfork is a common bifurcation. For example, the parameter values, $k_{\mathrm{sn}}(t)$, at which the first type t

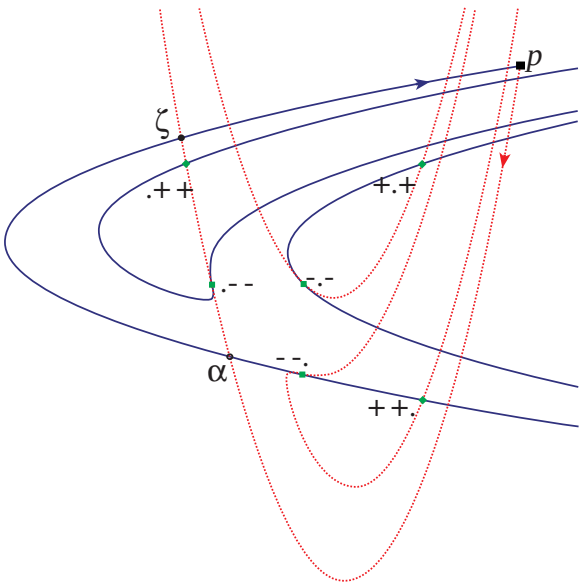

Figure 10: Stable and unstable manifolds for the $(+)^\infty$ fixed point of the Hénon map at $b = 1$ and $k = 3.09151$, where there is a cubic tangency of the manifolds at the $+^\infty - (--) - +^\infty$ homoclinic orbit.

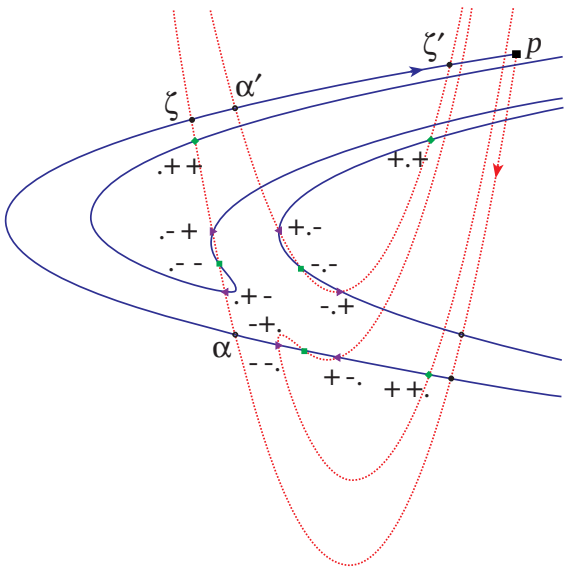

Figure 11: Type 2 homoclinic orbits of the Hénon Map at $k = 3.5$.

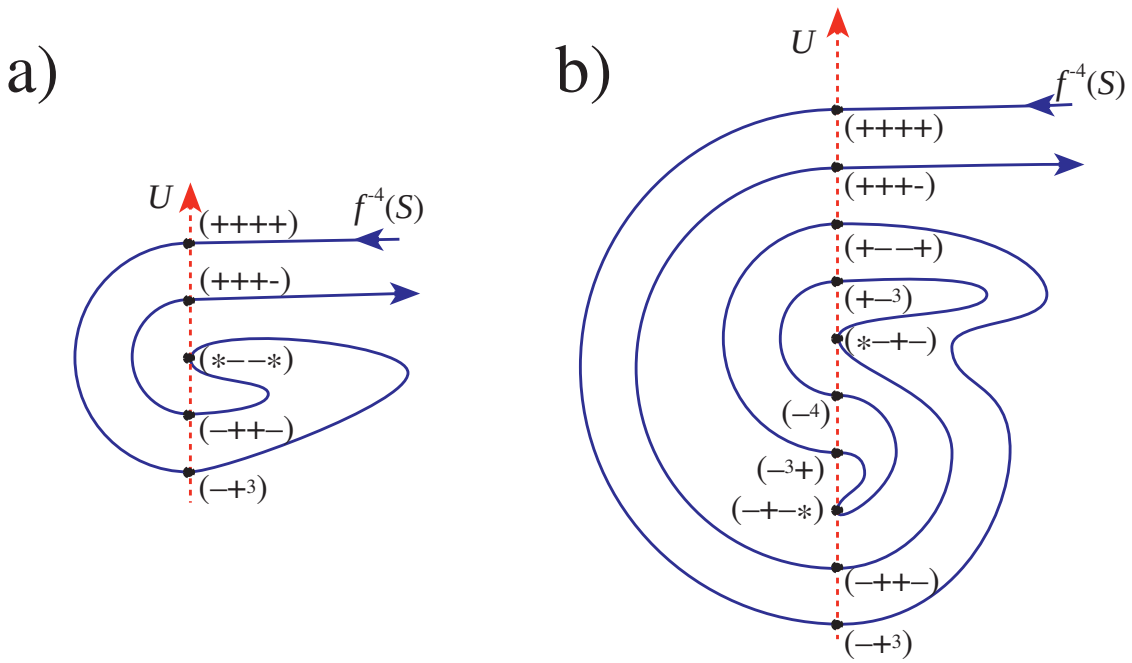

Figure 12: Sketch of two possible homoclinic saddle-node bifurcations of type four. A symmetric saddle-node creating $(*--*)$ occurs on $W^u((-++-),(+++*))$ in (a). An asymmetric saddle-node creating $(*-+-)$ and $(-+-*)$ occurs with one point on $W^u((-^4),(+--+))$ in (b).

homoclinic is created decrease monotonically with t. Thus at $k_{\rm sn}(t)$ the first type t orbit is born and there are no homoclinic orbits with type less than t. For $t > 1$, at $k_{\rm sn}(t-1)$ the segment $f^{t-1}(U)$ must intersect with S, so that $f^t(U)$ intersects with $f(S)$. In order for this to happen (when $b = 1$), there is a pitchfork bifurcation for $k_{\rm pf}(t) \in [k_{\rm sn}(t), k_{\rm sn}(t-1)]$ of the type t homoclinic orbit $+^\infty-(-+^{t-2}-)-+^\infty$ giving rise to the pair of orbits with symbol sequences

$$(-+^{t-2}-) \to {\rm pf}\{(-+^{t-1}),(+^{t-1}-)\}\,.$$

We see that the children of this bifurcation differ from their parent in a single symbol and they differ from each other in two symbols. Table 5 lists the first few such homoclinic bifurcation values obtained by extrapolation of the first few members of the approximating orbit sequence.

The distance (in k) between the birth of the transit time t orbit and its pitchfork bifurcation shrinks to zero as the transit time increases.

10 Intervals with no Bifurcations

Davis, MacKay and Sannami (DMS) [3] used the numerical method of Biham and Wenzel [16] to compute the periodic orbits for the area preserving Hénon

t	Core	$k_{\rm sn}(t)$	Pitchfork Children	$k_{\rm pf}(t)$
1	$(*)$	5.69931078670		
2	$(**)$	1.62777931098	$(-+), (+-)$	3.09150542113
3	$(*+*)$	0.38555621701	$(-+^2), (+^2-)$	0.71963023592
4	$(*+^2*)$	-0.13347378530	$(-+^3), (+^3-)$	-0.04427324816
5	$(*+^3*)$	-0.39678970175	$(-+^4), (+^4-)$	-0.36787481134
6	$(*+^4*)$	-0.54918558488	$(-+^5), (+^5-)$	-0.53740149261
7	$(*+^5*)$	-0.64623270965	$(-+^6), (+^6-)$	-0.64032496327
8	$(*+^6*)$	-0.71262572399	$(-+^7), (+^7-)$	-0.70916824264
9	$(*+^7*)$	-0.76055766670	$(-+^8), (+^8-)$	-0.75830622014
10	$(*+^8*)$	-0.79659407362	$(-+^9), (+^9-)$	-0.79501732767

Table 5: Pitchfork bifurcations from the first transit time orbits.

map. They showed that up to period 20, there are intervals of parameter where there appear to be no orbits created or destroyed. They studied a particular parameter interval near the destruction of the horseshoe, and elucidated the symbolic dynamics of the corresponding homoclinic tangle. We will refer to this interval as the DMS gap. Though the method of Biham and Wenzel is guaranteed to work close enough to the AI limit [6], it can fail [2]. We tested the DMS results using our continuation technique. The use of parallel computation allowed us to extend the original experiment by an order of magnitude in size so that we followed all orbits up to period 24—recall from Table 2 that there are a total of 1,465,020 possible orbits. We verify the DMS results and identify the symbol sequences of the orbits that form the boundaries of the DMS gap.

In our experiment we follow all orbits up to period 24 and record the parameter values at which they are destroyed. This list was sorted in increasing k order, and we plot the number of orbits present at each value of k. To reduce the size of the plot the data was smoothed so that all the orbits destroyed within a neighborhood of size Δk are counted together at the discretized value $n\Delta k$. The resulting plot of the number of periodic orbits as a function of k is shown in Fig. 13.

At the anti-integrable limit the map exhibits a horseshoe so all of the periodic orbits are present. As we move away from the anti-integrable limit we see a decline in the number of periodic orbits as orbits collide and are destroyed. Flat intervals in Fig. 13 represent intervals of parameter where very few bifurcations occur. Gaps in the plot indicate intervals of parameter where there are *no* bifurcations. The creation of the first type t homoclinic orbits gives rise to flat intervals. We observe that the left endpoint of each of the larger flat intervals for $k < 3$ corresponds to $k_{\rm sn}(t)$ for the saddle-node bifurcation of the first type t homoclinic orbits; these are marked in Fig. 13 and in the enlargement, Fig. 14. Similarly, the parameter values $k_{\rm pf}(t)$ are also marked; note that these pitchfork bifurcations are located well beyond the right endpoints of the flat intervals. Each of the flat intervals for $k < 3$

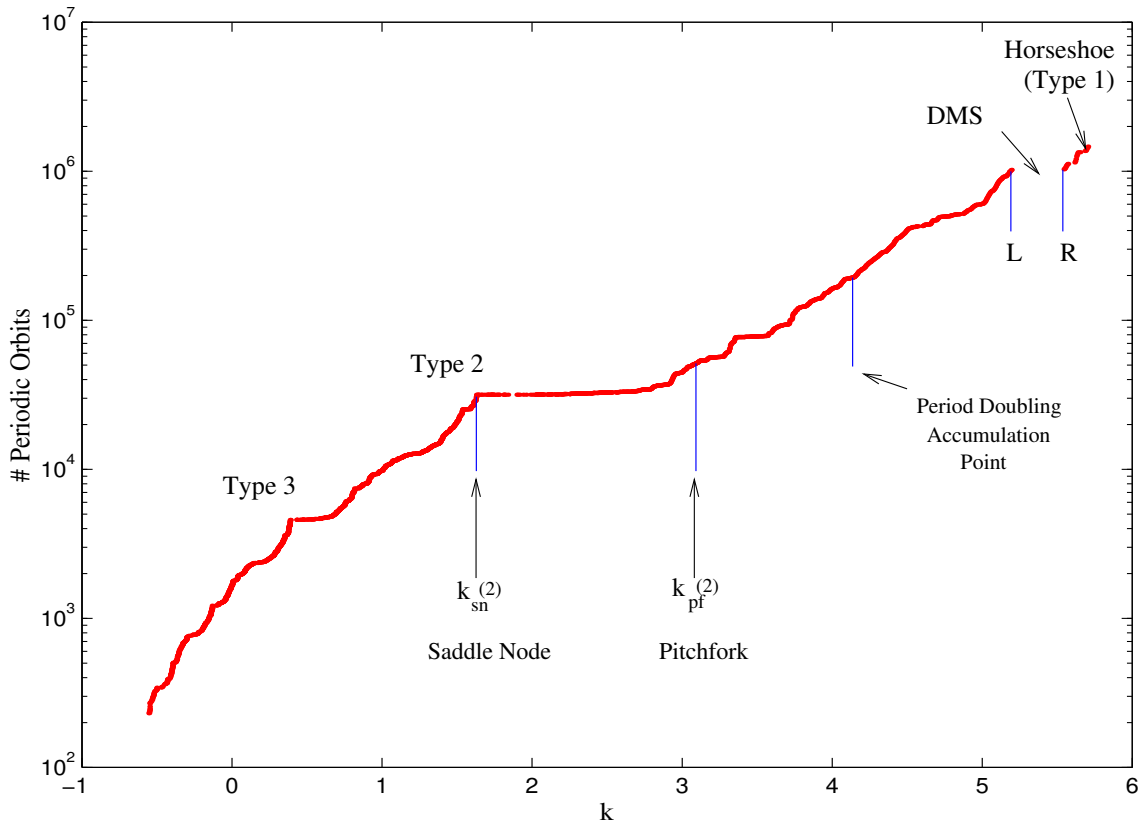

Figure 13: Number of periodic orbits of the Hénon map up to period 24, for $b = 1$, using $\Delta k = 7 \times 10^{-4}$. The maximal number is reached at $k \approx 5.69931078745$, when the horseshoe is formed. The endpoints of the largest gap studied by DMS are labeled by L and R.

must eventually fill in if we go to high enough period because in this range of k the area preserving Hénon map has an elliptic fixed point. Recall that an m/n bifurcation from the elliptic fixed point occurs at the parameter values $k_{m/n}$ given in Eq. (10), and these values are dense in the interval $-1 \leq k \leq 3$. Moreover, invariant circles bifurcate from the elliptic fixed point for each k_ω for sufficiently irrational ω. The same argument can be used up to the end of the period doubling cascade of the fixed point at $k \approx 4.13616680392$.

There are a number of distinct gaps in Fig. 13; the 3 larger gaps were studied by DMS, especially the largest one, near $k = 5.5$ indicated by L and R in Fig. 13. DMS conjecture that the dynamics in each gap is hyperbolic, and consequently there are no bifurcations in a gap. Our numerical evidence, which extends their study by an order of magnitude, supports this conjecture. Upon examining the orbits that limit on the endpoints of the gap up to period 24, we can extrapolate and find that each of the five largest gaps is bounded by a homoclinic bifurcation, see Table 6. Thus we see that the gaps do not fill-in with orbits converging on the homoclinic bifurcations,

Left Endpoint Core	k_L	Right Endpoint Core	k_R
$(-+-*-+-)$	4.55931896797	$(++-*-*-++)$	4.595679648027
$(+^3-+-*)$	4.84317164217	$(+^3-*-+-++-)$	4.867957620071
$(-+-*)$	5.18851121215	$(++-*-++)$	5.537656928123
$(-+++-*-+++-)$	5.56490867348	$(++-*-+^3)$	5.608721050386
$(-+++-*)$	5.63190980280	$(+^3-*-+^3)$	5.677692222290

Table 6: Homoclinic bifurcations bounding the gaps

but we cannot rule out that there are other, unrelated period orbits with period larger than 24 that are created at parameter values in the middle of a gap.

We observe that there are two types of bifurcations bounding the gaps: symmetric and asymmetric saddle-node bifurcations. The asymmetric saddle-nodes result in the creation of two pairs of homoclinic orbits, the one listed in the table, and its time-reverse. Typically we observe that symmetric saddle node bifurcations in homoclinic orbits are followed by pitchfork bifurcations. Surprisingly, only *one* of the symmetric saddle node endpoint sequences is followed by a pitchfork bifurcation. In fact we observe that among all of the homoclinic orbits through type 11, there are only 8 such special saddle-node bifurcations!

In Fig. 14 we show an enlargement of Fig. 13 but also include the data from the subshift, $\Sigma_{\mathcal{F}}$. In the upper right corner of Fig. 14 we see the tail end of the exit time 2 plateau. We also labeled the first large gap in $\Sigma_{\mathcal{F}}$ after the full subshift is destroyed—this is the subshift analog of the DMS gap.

As in the DMS gap, the left and right boundaries, denoted L and R, correspond to a pair of homoclinic saddle-node bifurcations with the core sequences

$$\begin{array}{ll} L & \operatorname{asn}\{(*+-++-),(-+++-+*)\} \\ R & \operatorname{sn}\{(+^3-+++-+^3),(+^3-^4+^3)\} \end{array} \tag{17}$$

These bifurcations occur at the extrapolated values

$$\begin{aligned} k_{\rm sn}(L) &\approx 1.533898312 \quad (\epsilon_{\rm sn}\approx 0.62821082)\,, \\ k_{\rm sn}(R) &\approx 1.583387630 \quad (\epsilon_{\rm sn}\approx 0.62216448)\,, \end{aligned}$$

respectively. Note that the right endpoint of the gap corresponds to an orbit whose partner is not in the subshift!

The curves for all orbits and for the subshift are remarkably similar and it appears that the growth of orbits in the subshift gives an accurate representation of the overall growth of orbits in the full shift for this range of parameters. This is especially remarkable given that fact when all the orbits exist, the subshift contains less than 1% of the orbits in the full shift up to period 24.

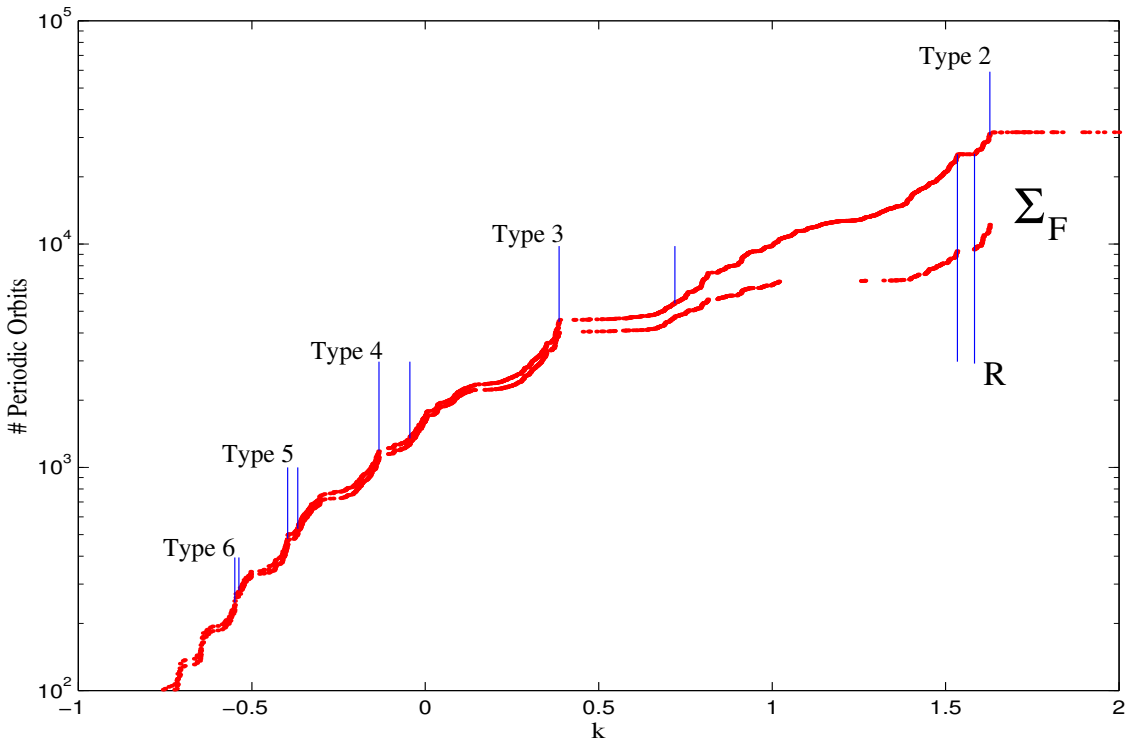

Figure 14: Enlargement: number of periodic orbits up to period 24 for the full shift and the subshift $\Sigma_{\mathcal{F}}$. The left and right ends of each plateau correspond to $k_{\rm sn}(t)$, and $k_{\rm pf}(t)$.

The figure shows that for small k, the number of orbits in the full shift is nearly a constant multiple of that in the subshift.

11 Conclusions

Continuation from an anti-integrable limit is an effective technique for studying orbits providing that there are no isolated bubbles in the bifurcation diagram. Since the Hénon map has as most 2^n fixed points of period n, which is the number of orbits that exist in the AI limit, this hypothesis is at least reasonable for this case, but we know of no proof. In [6] we applied the anti-integrable theory to the Hénon map to obtain a new proof of the well-known analytical bound of Devaney and Nitecki [5]. In Thm. 2 we applied a similar argument to a restricted set of orbits to find an analytical bound for the destruction of a subshift of finite type. We presented both analytical bounds together with the optimal bounds generated numerically using our continuation method. We observed that the horseshoe was destroyed by a type one bifurcation that was homoclinic in the area preserving case , and heteroclinic otherwise . In either case we conjectured that this bifurcation

was the first bifurcation among *all* orbits of the Hénon map as we receeded from the anti-integrable limit.

With our continuation method, we were able to assign a "global code" to each orbit, by fixing the designation as that at the AI limit. In the Hénon map, we demonstrated that these AI codes are equivalent to the standard horseshoe code (when it exists), but they also give a consistent way of assigning symbols to orbits *beyond* the destruction of the horseshoe. Remarkably, there appears to be a relationship between the AI codes for a number of systems including billiards, twist maps of the cylinder and the Hénon map. We will explore this relationship in a forthcoming paper [21].

In studying homoclinc orbits we related the properties *transit time*, *type*, and *signature* to properties of the core of a homoclinic orbit. We also demonstrated that the ordering of the homoclinic orbits on the manifold segments U and S is the standard unimodal ordering. The notion of *double neighbors* and lemmas 7 and 8 gave criteria for a pair of homoclinic orbits to bifurcate. Surprisingly, these also gave a forcing relation that tells us which homoclinic bifurcations are forced by other homoclinic bifurcations. Having shown that homoclinic bifurcations can only take place between *double neighbors* with the same core length, Lem. 10 gave a symbolic criterion for a pair of homoclinc orbits to be neighbors. If the symbolic ordering persists after the horseshoe was destroyed one could start to predict which homoclinic orbits must bifurcate using only the symbolic labeling derived from the AI code. The ordering is certainly valid until the horseshoe is destroyed, which lead to a theorem that the first homoclinic bifurcation of the hyperbolic fixed point in the area preserving Hénon map occurs between the pair of type one orbits. In the area preserving case the Hénon map has a symmetry and we discussed the mechanism by which pitchfork and asymmetric saddle node bifurcations occur.

With our continuation technique we computed numerical values for various bifurcations of the homoclinic orbits up to type eleven. We hand-sketched the bifurcation diagram at type three, but then used a simple algorithm on the computer to construct the much more complex figures for higher core length. In contrast to our method, the Biham and Wenzel [17, 39] method for finding orbits is known to fail in certain cases [2], and can only be justified in the neighborhood of a two symbol AI limit [6]. Nevertheless, for the area-preserving Hénon map, we observed precisely the same number of orbits using our technique as was reported by DMS using the Biham-Wenzel method [3]. We extended the original experiment of DMS in two ways. First, we studied an order of magnitude more orbits than the original experiment and yet the gaps originally reported by DMS persisted. We observed that homoclinic bifurcations are responsible for these gaps and we listed the symbolic labels of the orbits that form the gap endpoints in Table 6. These gaps correspond to the creation and destruction of parameter intervals where the dynamics of the area-preserving Hénon map appears to be conjugate to a subshift of finite type. After extending the size of the

original experiment we extracted the $\Sigma_{\mathcal{F}}$ orbits from our data. We found a similar gap structure in the subshift data and listed the symbolic labels for the homoclinic orbits that form the endpoints of the gap that is the analog of the DMS gap. Having observed that the gaps are bounded by homoclinic orbits, we regenerated the orbit growth plot using *only* homoclinic orbits. As expected, the gap structure and overall shape of Fig. 13 were almost completely captured by the homoclinic orbits alone.

References

[1] R.W. Easton. Trellises formed by stable and unstable manifolds in the plane. *Trans. Am. Math. Soc.*, 294(2):719–732, 1986.

[2] P. Grassberger, H. Kantz, and U. Moenig. On the symbolic dynamics of the Hénon map. *J Phys A*, 22(24):5217–5230, 1989.

[3] M.J. Davis, R.S. MacKay, and A. Sannami. Markov shifts in the Hénon family. *Physica D*, 52:171–178, 1991.

[4] S. J. Aubry. The concept of anti-integrability: Definition, theorems and applications to the standard map. *Twist Mappings and their Applications, Ed Richard McGehee, Kenneth R. Meyer*, pages 7–54, 1992.

[5] R.L. Devaney and Z. Nitecki. Shift automorphisms in the Hénon mapping. *Commun. Math. Phys.*, 67:137–146, 1979.

[6] D. Sterling and J.D. Meiss. Computing periodic orbits using the anti-integrable limit. *Physics Letters A*, 241:46–52, 1998.

[7] Rüdiger Seydel. *Practical Bifurcation and Stability Analysis from Equilibrium to Chaos, 2nd Ed.* Springer-Verlag, 1992.

[8] P Cvitanovic, G.H. Gunaratne, and I. Procaccia. Topological and metric properties of Hénon type strange attractors. *Phys. Rev. A*, 38:1503–1520, 1988.

[9] Bai-lin Hao. Symbolic dynamics and characterization of complexity. *Phyica D.*, 51:161–176, 1991.

[10] K.T. Hansen. Remarks on the symbolic dynamics for the Hénon map. *Phys. Lett. A*, 165:100–104, 1992.

[11] F. Christiansen and A. Politi. Symbolic encoding in symplectic maps. *Nonlinearity*, 9:1623–1640, 1995.

[12] S.E. Newhouse. Quasi-elliptic periodic points in conservative dynamical systems. *Am. J. Math.*, 99:1061–1087, 1977.

[13] N. Gavrilov and L. Silnikov. On the three dimensional dynamical systems close to a system with a structurally unstable homoclinic curve, i. *Math. USSR Sbornik*, 17:467–485, 1972.

[14] N. Gavrilov and L. Silnikov. On the three dimensional dynamical systems close to a system with a structurally unstable homoclinic curve, ii. *Math. USSR Sbornik*, 19:139–156, 1973.

[15] C. Robinson. Bifurcation to infinitely many sinks. *Comm. Math. Phys.*, 90:433–459, 1983.

[16] O. Biham and W. Wenzel. Characterization of unstable periodic orbits in chaotic attractors and repellers. *Phys. Rev. Lett.*, 63:819–822, 1989.

[17] O. Biham and W. Wenzel. Unstable periodic orbits and symbolic dynamics of the complex Hénon map. *Phys. Rev. A*, 42:4639–4646, 1990.

[18] S. J. Aubry. Anti-integrability in dynamical and variational problems. *Physica D*, 86:284–296, 1995.

[19] R.S. MacKay and J.D. Meiss. Cantori for symplectic maps near the anti-integrable limit. *Nonlinearity*, 5:149–160, 1992.

[20] S. Aubry and G. Abramovici. Chaotic trajectories in the standard map, the concept of anti-integrability. *Physica D*, 43:199–219, 1990.

[21] H. Dullin, D. Sterling, and J.D. Meiss. Global symbolic codes for maps. *In Progress*, 1998.

[22] H.B Keller. *Numerical Methods in Bifurcation Problems*. Published for the Tata Institute by Springer-Verlag, 1997.

[23] J.D. Meiss. Symplectic maps, variational principles, and transport. *Reviews of Modern Physics*, 64(3):795–848, 1992.

[24] R.S. MacKay and J.D. Meiss. Linear stability of periodic orbits in Lagrangian systems. *Phys. Lett. A*, 98:92–94, 1983.

[25] John Smillie. Complex dynamics in several variables. In *Flavors of geometry*, volume 31 of *Math. Sci. Res. Inst. Publ.*, pages 117–150. Cambridge University Press, Cambridge, 1997. With notes by Gregery T. Buzzard.

[26] M. Benedicks and L. Carleson. The dynamics of the henon map. *Annals of Mathematics*, 133:73–169, 1991.

[27] R.S. MacKay, J.D. Meiss, and I.C. Percival. Resonances in area preserving maps. *Physica D*, 27:1–20, 1987.

[28] R.W Easton. *Geometric Methods for Discrete Dynamical Systems*. Oxford University Press, 1998.

[29] J.D. Meiss. Average exit time for volume preserving maps. *Chaos*, 7:139–147, 1997.

[30] V. Rom-Kedar. Homoclinic tangles-classification and applications. *Nonlinearity*, 7:441–473, 1992.

[31] J. H. Curry and J.R. Johnson. On the rate of approach to homoclinic tangency. *Phys. Lett. A*, 92(5):217–219, 1982.

[32] S. Newhouse. Diffeomorphism with infinitely many sinks. *Topology*, 13:9–18, 1974.

[33] R. Rimmer. Symmetry and bifurcation of fixed points of area-preserving maps. *J. Diff. Eqns*, 29:329–344, 1978.

[34] J.S.W.Lamb, editor. *Time-Reversal Symmetry in Dynamical Systems*, volume 112 of *Physica D*, Amsterdam, 1998. Elsevier.

[35] R.S. MacKay. *Renormalisation in Area-Preserving Maps*, volume 6 of *Advanced Series in Nonlinear Dynamics*. World Scientific, Singapore, 1993.

[36] J.W.S. Lamb and J.A.G. Roberts. Time-reversal symmetry in dynamical systems: A survey. *Physica D*, 112:1–39, 1998.

[37] R.L. Devaney. *Introduction to Chaotic Dynamical Systems*. Addison-Wesley, 1989.

[38] Vered Rom-Kedar. Secondary homoclinic bifurcation theorems. *Chaos*, 5(2):385–401, 1995.

[39] W. Wenzel, O. Biham, and C. Jayaprakash. Periodic orbits in the dissipative standard map. *Physical Review A*, 43:6550–6567, 1991.